batteries

MDPI

Article

Economic Optimization of Battery Storage for Power Ramp- Rate Control and Energy Arbitrage in PV and Wind Power Systems

Rodolfo Dufo-López *, Juan M. Lujano-Rojas and José L. Bernal-Agustín

Department of Electrical Engineering, Universidad de Zaragoza, 50018 Zaragoza, Spain; lujano.juan@unizar.es (J.M.L.-R.); jlbernal@unizar.es (J.L.B.-A.)
* Correspondence: rdufo@unizar.es; Tel.: +34-876555124

Abstract

With the increasing renewable penetration in electrical grids, high power ramp rates can lead to grid instability. Power ramp-rate control (PRRC) requirements are being implemented in an increasing number of countries, with penalties for non-compliance. While curtailment and power reservation enable ramp-rate control without energy storage, they inherently decrease the grid-injected energy and generation revenue. Battery storage avoids these drawbacks while reducing violations, and can also be used for arbitrage to increase profitability. This study proposes a simulation-based optimization framework to maximize the net present value (NPV) of battery storage integrated into PV, wind, and hybrid PV–wind systems under two distinct penalty schemes. A battery-based PRRC is compared with curtailment and power reserve strategies, revealing that battery storage yields the highest NPV and the fewest ramp-rate violations. Using Spain's 2025 hourly electricity market prices and current utility-scale battery costs, the system with an LTO (high C-rate) battery-based PRRC under a 10%/min ramp-rate limit achieves an NPV comparable to the unconstrained case. Battery arbitrage under these conditions is not worthwhile, as the NPV improvement is negligible. Under a hypothetical stretched price scenario (average price: 102.9 EUR/MWh; average daily spread: 232.1 EUR/MWh), energy arbitrage using an LFP battery (low C-rate) becomes highly profitable. Relative to the unconstrained baseline, this strategy yields net present value (NPV) improvements of 17% for the wind system and 28% for the hybrid PV–wind system. Furthermore, the NPV for the PV system shifts from −2 million EUR to 6 million EUR, demonstrating that arbitrage viability depends heavily on market price volatility.

Keywords: power ramp rate; battery; energy arbitrage; photovoltaic; wind turbine; curtailment; power reserve; economic optimization

Check for updates

Received: 11 September 2026
Revised: 13 October 2026
Accepted: 14 October 2026
Published: 16 October 2026

Copyright: © 2026 by the authors. Licensee MDPI, Basel, Switzerland. This article is an open access article distributed under the terms and conditions of the Creative Commons Attribution (CC BY) license.

1. Introduction

With the increasing renewable penetration in electrical grids, traditional generators are being replaced by low-inertia renewable systems connected through power converters. Furthermore, renewable generators typically operate at maximum available power, without power reserves [1]. The intermittent nature of renewable power, the reduction in inertia, and the decrease in power reserves can lead to power and voltage fluctuations and frequency stability problems [1,2].

Rapidly passing clouds over large photovoltaic (PV) systems can cause high variations in output power (instances exceeding 50% of rated power in less than 10 s have been reported [3]), producing high power ramp rates. In wind farms, drastic changes in wind

speed over short periods can also produce high power fluctuations and, therefore, high ramp rates [4,5]. Hybrid PV–wind systems can lead to a reduction in ramp rates [6], but ramp-rate issues may persist in some cases. Different transmission system operators (TSOs) require power ramp-rate control (PRRC) capability of PV and wind generators [7] to reduce the number of power ramp-up and ramp-down events (violations of maximum admissible limits). The ramp-rate limits established by the TSOs of different countries (Puerto Rico, Germany, Denmark, Mexico, Ireland, Hawaii, and China) are usually specified as a percentage of rated power variation per unit time (e.g., 10%/min in Puerto Rico) or as the power variation per time step (e.g., 2 MW/min in Hawaii), and can differ for ramp-up and ramp-down rates.

Different approaches have been applied for PRRC. In PV systems, several reviews of different methods have been published [8–11]. Battery storage for PRRC is typically managed through control algorithms, such as the moving average, exponential smoothing, filter-based, and ramp-rate-based methods, each with their own advantages and limitations [8]. Li-ion batteries are generally considered the most suitable storage technology for PRRC [12]. In [13], the researchers concluded that, for PRRC, battery power (rated power of the inverter–charger) is more critical than battery capacity. For ramp-up events, power curtailment methods are used to reduce violations. Although curtailment has a low implementation cost, it wastes energy and therefore reduces revenue from energy sales compared to storage-based approaches. For ramp-down violation mitigation, power reserve can be used without storage, but it also results in energy waste (e.g., zero violations were reported with a 20% PV power reserve in [3]).

While the above discussion focuses on PV systems, similar challenges arise in wind power. Regarding wind power systems, two main groups of PRRC techniques exist [14]: turbine techniques and storage techniques. Turbine techniques (blade pitch control and rotor inertia control, used for curtailment and/or power reserve to reduce ramp-up and ramp-down violations) have significant limitations in power ramp-rate reduction and result in energy waste. Storage techniques, typically batteries, have been widely studied [15–17], although other technologies, such as pumped hydro storage [4], ultracapacitors, and hybrid storage [18], have also been proposed. Storage provides maximum flexibility and power ramp-rate reduction compared to turbine-based techniques. A review of different storage technologies for mitigating wind power fluctuations [19] identified Li-ion batteries as the most suitable technology for wind fluctuation stability in general, and for PRRC in particular. For hybrid PV–wind power systems, similar PRRC techniques have been applied [18,20]. Figure 1 illustrates an example of a PV system output with a 10%/min ramp-rate limit, shown without PRRC and with battery-based PRRC.

Beyond PRRC, batteries can also be used for energy arbitrage (storing renewable energy during low electricity price periods and injecting it into a grid during peak price periods). The profitability of an arbitrage system depends on the storage costs, battery degradation, and the hourly electricity pricing profile [21–26].

To the best of the authors' knowledge, no previous study has performed a systematic economic optimization comparing all major PRRC strategies—curtailment, power reserve, and battery storage—under real market conditions while simultaneously considering battery arbitrage. This paper addresses this gap.

This work demonstrates the application of batteries in PV, wind, and hybrid PV–wind power generation systems to comply with ramp-rate limitations. The performance and economic parameters are compared across different PRRC scenarios (curtailment, power reserve, combined curtailment with power reserve, and battery with curtailment). For the battery case, the option of energy arbitrage is also considered. Unlike previous works, the effect of battery ageing is accurately modeled—accounting for depth of discharge,

state of charge, C-rate, and temperature effects on both cycling and calendar ageing—and incorporated into the economic calculations. A new decision tree is developed to define the priorities for using battery charging/discharging, curtailment, and power reserves to comply with ramp-rate limitations. Furthermore, this study is the first to simultaneously consider battery storage for arbitrage and ramp-rate control, evaluate its economic performance, and compare it against other PRRC strategies under a unified economic framework.

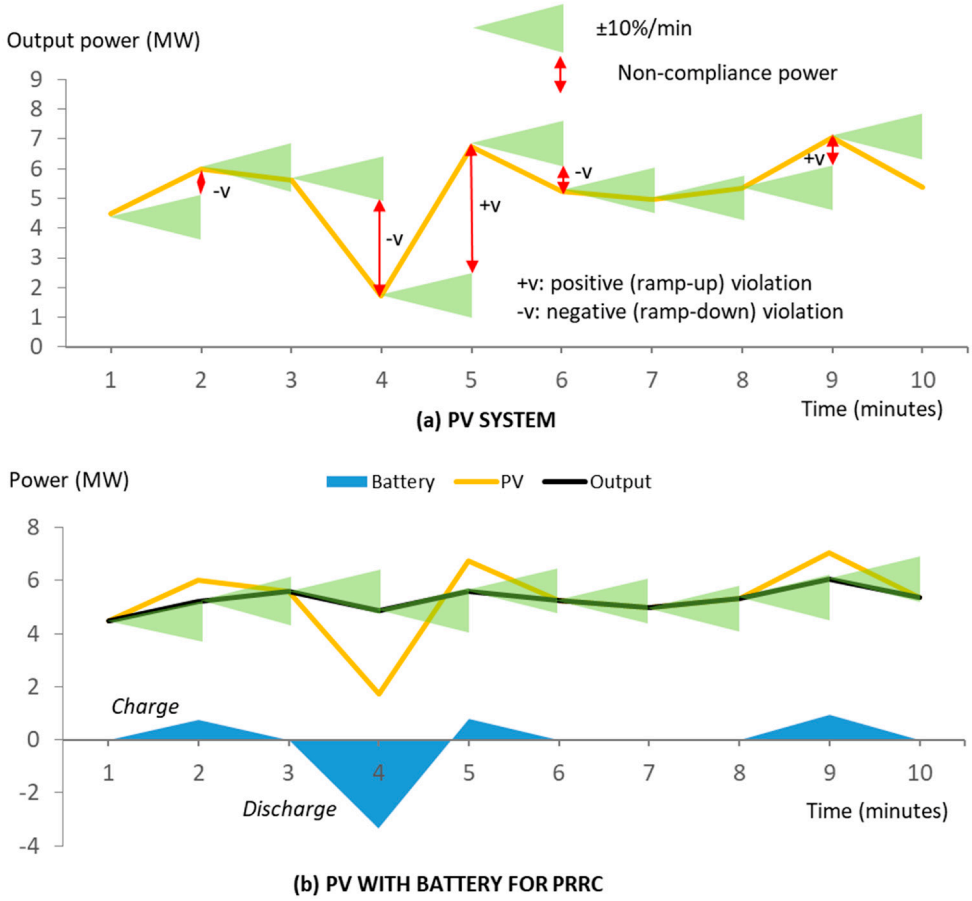


Figure 1. PV system of 7.2 MW rated power. Performance over 10 min. (**a**) PV system without PRRC (5 violations); (**b**) PV system with battery for PRRC (no violation).

To synthesize these objectives within a unified scientific framework, this study tests the central hypothesis that co-optimizing battery storage for joint energy arbitrage and ramp-rate control yields higher net economic profitability than non-storage PRRC strategies (curtailment and/or power reserves) under some conditions. The proposed decision tree dispatch strategy, detailed battery aging formulation, and multi-scenario evaluations serve as the unified analytical framework required to map these economic trade-offs and identify the optimal operational boundaries across PV, wind, and hybrid power plants.

The remainder of this paper is organized as follows: Section 2 describes the system model and optimization methodology; Section 3 validates the model by comparing its results against previously published works, presents the case study and simulation scenarios and discusses the results; and Section 4 draws the main conclusions.

2. Materials and Methods

Figure 2 shows the utility-scale renewable power system studied in this work: a PV, wind, or hybrid PV–wind system, with or without battery storage. The simulation and

optimization were performed using the MHOGA software (MegaWatt Hybrid Optimization by Genetic Algorithms, version 4.0, University of Zaragoza, Zaragoza, Spain).

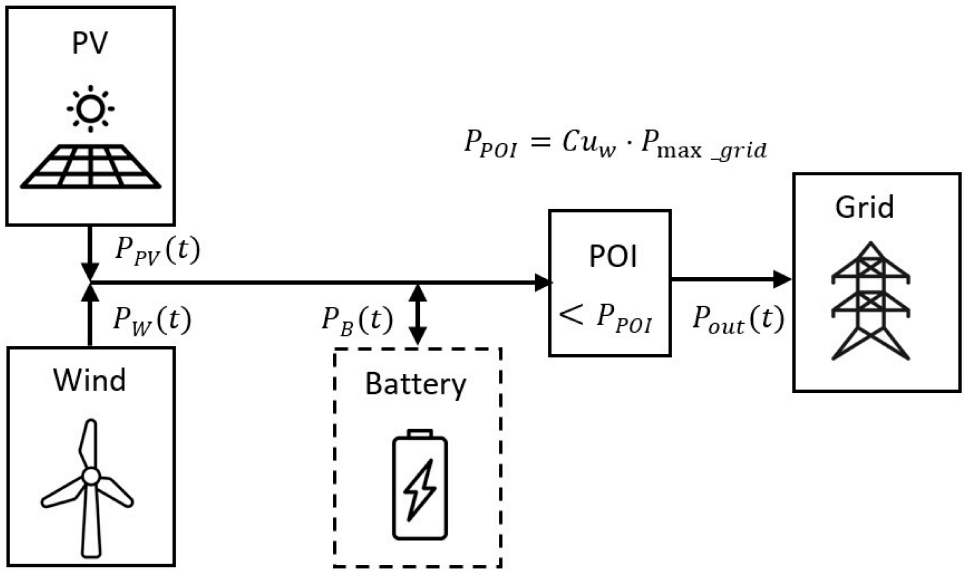


Figure 2. Components and power of the system.

2.1. Power Ramp Rate

The power ramp rate RR (%/min) is defined as the percentage of the system's nominal power variation per unit time [27]:

$$RR = \frac{100 \cdot [P_{out}(t) - P_{out}(t - \Delta t)]}{P_{POI} \cdot \Delta t} \quad (1)$$

where $P_{out}(t)$ (MW) is the output power (injected into the grid) at a given instant t, $P_{out}(t - \Delta t)$ is the output power at the previous time step, P_{POI} is the maximum power allowed by the grid operator at the point of interconnection (POI), and Δt (min) is the time interval of the ramp-rate calculation (Δt = 1 min in this work).

A 1 min time step represents the sweet spot for annual renewable energy simulations, offering the ideal balance between capturing fast power transients and maintaining computational feasibility: a 1 min resolution keeps full-year data arrays (525,600 steps) manageable for complex optimization algorithms [13]; grid operators worldwide define active power ramp-rate constraints over 1 min time windows [14,28]; high-quality solar irradiance and wind speed measurement networks standardly capture variability at 1 min sampling intervals, making 1 min the benchmark resolution for empirical smoothing models without introducing artifacts from interpolation [20]; physical BESS sizing, state-of-charge tracking, and active power ramp management operate on minute-level time horizons [29]; and 1 min interval data successfully captures the primary power fluctuations and peak ramp events driven by cloud movement and wind gusts, providing sufficient accuracy for sizing smoothing systems over full-year horizons [20].

P_{POI} is equal to the maximum power allowed by the grid operator ($P_{\max_grid}$), unless a curtailment has been imposed as a penalty for previous ramp-rate violations:

$$P_{POI} = Cu_w \cdot P_{max_grid} \quad (2)$$

where Cu_w is the curtailment factor imposed by the grid operator (1 if no curtailment is imposed). The subscript "w" denotes "weekly", as in the limiting maximum POI

power penalty system [27], where P_{POI} is updated weekly by the curtailment factor Cu_w (Section 2.2.1).

The output power of the system $P_{out}(t)$ (MW) (Figure 2) is calculated as

$$P_{out}(t) = min(P_{PV}(t) + P_W(t) - P_B(t), P_{POI}) \quad (3)$$

where $P_{PV}(t)$ and $P_W(t)$ are the PV and wind power, and $P_B(t)$ is the battery power (positive for charging, negative for discharging).

If the ramp rate is positive and exceeds a specific limit RR_{up_max} (%/min), a ramp-up violation occurs:

$$P_{out}(t) - P_{out}(t - \Delta t) > 0 \bigwedge RR > RR_{up_max} \Longrightarrow Ramp_up\ violation \quad (4)$$

If a negative ramp rate exceeds the limit RR_{dow_max}, a ramp-down violation occurs:

$$P_{out}(t) - P_{out}(t - \Delta t) < 0 \bigwedge |RR| > RR_{down_max} \Longrightarrow Ramp_down\ violation \quad (5)$$

For example, the Nordic Grid Code and the Puerto Rico Electric Power Authority establish a limit of $RR_{up_max} = RR_{up_min} = 10\%/\text{min}$ [15].

2.2. Penalty for Ramp-Rate Violations

Two different penalty policies are considered in this work.

2.2.1. Limiting Maximum POI Power Penalty System

The maximum power at the point of interconnection P_{POI} is updated on a weekly basis, following the regulatory framework in Puerto Rico [27], although alternative update intervals can also be considered. If the number of ramp-rate violations during a week exceeds a maximum value, the P_{POI} is reduced the following week as a penalty, reducing the energy injected into the grid and therefore reducing revenue. This penalty system works as follows [27].

For each week, the number of ramp-rate violations NV_W in 1 min time steps (ramp-up plus ramp-down violations) is counted.

For each week, the ramp-rate compliance index RRC_w (%) is calculated using Equation (6):

$$RRC_W = 100\left(1 - \frac{NV_W}{W \cdot 24 \cdot 60}\right) \quad (6)$$

where W is the number of days in the period for updating the POI maximum power (the default value in Puerto Rico is $W = 7$ days, or one week).

A minimum RRC value is defined to avoid curtailment penalties (accounting for metering accuracy, tolerance, etc.), denoted as RRC_{W_min} (98.5% in Puerto Rico). If the RRC_w in a given week falls below the RRC_{W_min}, the grid operator imposes a curtailment factor Cu_W for the following week, calculated as

$$Cu_W = min\left(1, Cu_{W-1} - \left(\frac{RRC_{W_min} - RRC_{W-1}}{100}\right)\right) \quad (7)$$

where Cu_{W-1} and RRC_{W-1} are the respective values from the previous week. The maximum power that can be injected into the grid (P_{POI}) is updated for week w using Cu_W in Equation (2).

This penalty system can readily be adapted to time periods other than one week by replacing W in Equation (6) with the actual number of days in the selected period.

2.2.2. Fee Penalty System

This penalty scheme applies a fee for the energy involved in ramp-rate violations [30]. The annual penalty cost is calculated as

$$C_{penalty} = \sum_{t=0}^{T_m} P_{NC}(t) \cdot \Delta t_h \cdot p_{fee}(t) \quad (8)$$

where T_m = 525,600 is the number of 1 min time steps per year, $P_{NC}(t)$ (MW) is the non-compliance power at each time step (power excess or deficit during a ramp-up or ramp-down violation), Δt_h = 1/60 h is the time step in hours, and $p_{fee}(t)$ is the penalty fee (EUR/MWh).

The annual non-compliance energy E_{NC} (MWh) is calculated as

$$E_{NC} = \sum_{t=0}^{T_m} P_{NC}(t) \cdot \Delta t_h \quad (9)$$

2.3. Scenarios for PRRC

To reduce ramp-rate violations and avoid penalties, different PRRC techniques are considered: curtailment and/or power reserve of the generated power, and battery storage with curtailment (curtailment is only used when the battery cannot eliminate the ramp-up violation). Additionally, the case of battery storage (with curtailment) for PRRC while also considering energy arbitrage is evaluated.

First, the system is simulated without PRRC in 1 min time steps over a full year, evaluating both the technical performance (annual energy injected into the grid, number of ramp-rate violations, etc.) and economic performance (NPV and levelized cost of energy, LCOE). The different PRRC strategies are then considered and evaluated under the scenarios shown in Figure 3.

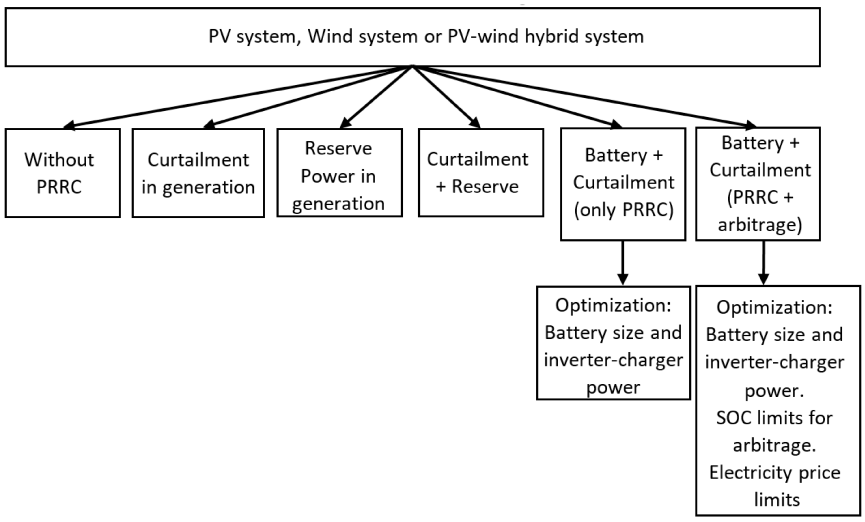


Figure 3. Different PRRC scenarios to be evaluated.

For comparative purposes, the power system without ramp-rate limitations (unconstrained case) is also evaluated.

The performance of the storage system can be assessed using the abatement ratio *AR* (%) [15], which compares the total number of violations occurring during the year (*NV*) in the case without PRRC against the case with storage:

$$AR = 100\left(1 - \frac{NV_{with\ storage}}{NV_{without\ PRRC}}\right) \tag{10}$$

Other authors [27] evaluated PRRC performance using the percentage of exported energy $EE_{\%}$ (%): the annual energy exported to the grid, EE (GWh/yr), relative to the energy exported in the case without ramp-rate limitation (unconstrained case).

$$EE_{\%} = 100\left(\frac{EE}{EE_{without\ ramp-rate\ limitation}}\right) \tag{11}$$

The ramp-rate compliance RRC (%) can also be used to evaluate PRRC performance [27].

$$RRC = 100\left(1 - \frac{NV}{T_m}\right) \tag{12}$$

2.4. Economic Evaluation

For each system and scenario, the NPV (in EUR) is calculated by considering the present value of revenues and costs over the system lifetime [26].

$$NPV = \sum_{y=1}^{Y} I_E \frac{(1+Inf_{Pr})^y}{(1+I)^y} - \sum_j \left(CAPEX_j + NPC_{rep_j} + \sum_{y=1}^{Y}\left(\frac{(OPEX_j + C_{penalty})(1+Inf)^y}{(1+I)^y}\right)\right) \tag{13}$$

where I_E (in EUR) is the annual revenue from electricity sales to the grid, Y is the system lifetime (years), I is the annual nominal discount rate (interest rate), and Inf_{Pr} is the expected electricity price inflation rate. The costs include capital expenditures ($CAPEX_j$), annual operational expenditures ($OPEX_j$), and penalty cost ($C_{penalty}$) where applicable, all escalated at the annual general inflation rate (Inf), as well as the net present cost of replacements (NPC_{rep_j}) over the system lifetime for all components j (PV generator, wind turbines, battery and inverter–charger).

The annual revenue is calculated as

$$I_E = \sum_{t=0}^{T_m} P_{out}(t) \cdot \Delta t_h \cdot Pr(t) \tag{14}$$

where $Pr(t)$ (in EUR/MWh) is the electricity price at time step t.

The $LCOE$ (in EUR/MWh) is calculated as

$$LCOE = \frac{ACS}{EE} \tag{15}$$

where ACS (in EUR) is the annualized system cost and EE (MWh/yr) is the annual energy injected into the grid.

$$ACS = NPC \cdot CRF \tag{16}$$

$$E_{out} = \sum_{t=0}^{T_m} P_{out}(t) \cdot \Delta t_h \tag{17}$$

where NPC (in EUR) is the total net present cost over the system lifetime and CRF is the capital recovery factor.

$$CRF = \frac{r(1+r)^Y}{(1+r)^Y - 1} \tag{18}$$

where r is the annual real discount rate,

$$r = \frac{I - Inf_{Pr}}{1 + Inf_{Pr}} \quad (19)$$

Note that different inflation rates are applied to revenues (Inf_{Pr}, annual electricity price escalation rate) and operational costs (Inf, general inflation) to reflect the distinct price dynamics of electricity markets and O&M costs.

2.5. Optimization

The objective of the optimization is the maximization of the NPV.

$$max(NPV) \quad (20)$$

In the scenarios with batteries, the optimizable parameters are as follows (search space defined in Section 3):

- Battery rated capacity C_B (MWh).
- Inverter–charger rated power $P_{I/Ch}$ (MW).

The battery duration T_B (h) is obtained from Equation (21), while the nominal C-rate is the inverse.

$$T_B = \frac{C_B}{P_{I/Ch}} \quad (21)$$

The full allowable battery state-of-charge (SOC) range is used for PRRC: between the minimum SOC_{min} (%) and the maximum SOC_{max} (%).

In the scenarios with energy arbitrage, four additional variables are optimized (search space defined in Section 3):

- The SOC limits for energy arbitrage (minimum and maximum SOC allowed for arbitrage, SOC_{A_min} and SOC_{A_max}, light-blue zone in Figure 4), defining the upper and lower buffer SOC zones reserved exclusively for PRRC (dark-blue zones).
- The highest and lowest electricity price allowed for charging and for discharging, respectively, $Pr_{A_High_C}$ and $Pr_{A_Low_D}$ (in EUR/MWh).

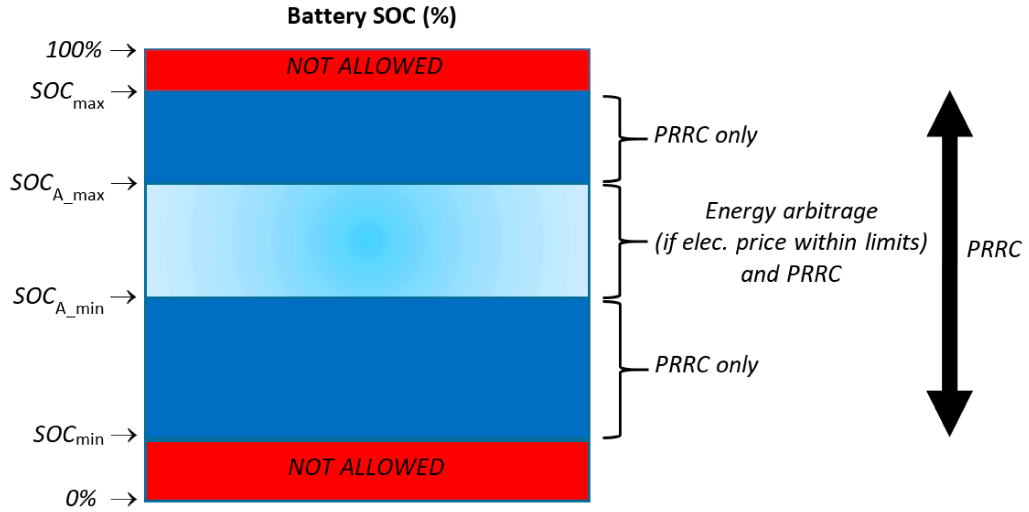


Figure 4. Battery SOC limits for PRRC and for energy arbitrage.

The optimization is carried out using the meta-heuristic Genetic Algorithm (GA) method (see Section 3 for implementation details).

2.6. Simulation of the System

Figure 5 shows the flowchart for the simulation of each scenario in 1 min time steps over a full year.

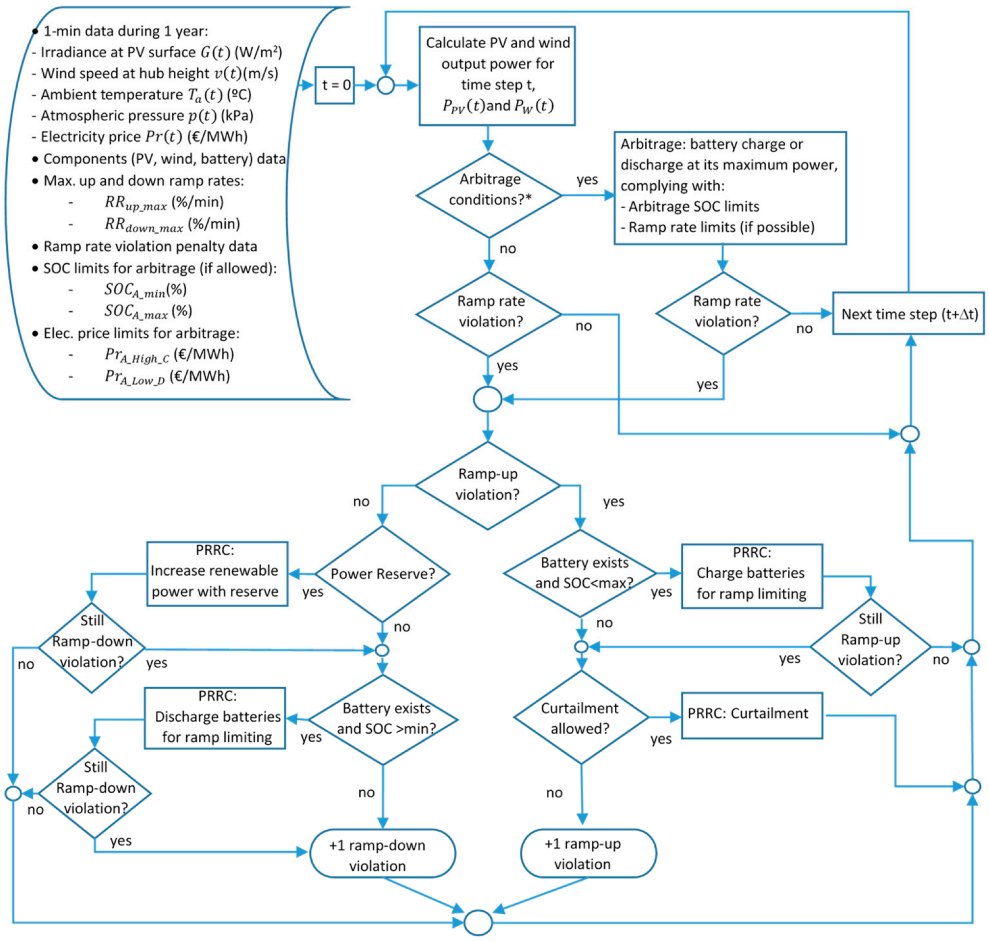


Figure 5. Flowchart of the decision tree for system dispatch and ramp-rate control during the annual 1 min time-step simulation.

If arbitrage is considered, the arbitrage conditions (marked with * in Figure 5) are as follows:

$$SOC(t) > SOC_{A_min} \bigwedge SOC(t) < SOC_{A_max} \tag{22}$$

$$Pr(t) < Pr_{E_High_C} \Longrightarrow Charge\ (arbitrage) \tag{23}$$

$$Pr(t) > Pr_{E_Low_D} \Longrightarrow Discharge\ (arbitrage) \tag{24}$$

Charging by arbitrage occurs when conditions (22) and (23) are simultaneously satisfied, while discharging occurs when conditions (22) and (24) are simultaneously satisfied.

The performance models of the different components are described in the following subsections.

2.6.1. PV Generator Performance

The AC output power of the PV generator at time step t, $P_{PV}(t)$ (W), is given by Equation (25):

$$P_{PV}(t) = \min\left(\eta_{Inv_{PV}} P_{PV_{N_{DC}}} \cdot \frac{G(t)}{G_{ref}} \cdot f_{PV_{loss}} \left[1 + \frac{\alpha}{100} \cdot \left(T_c(t) - T_{c_{ref}}\right)\right],\ P_{Inv_PV_N}\right) \tag{25}$$

where $G(t)$ is the irradiance over the PV surface (W/m^2); $T_c(t)$ is the average cell temperature (°C); η_{inv_PV} and $P_{Inv_PV_N}$ are the PV inverter efficiency (variable with power) and rated inverter power (W), respectively. $P_{PV_N_DC}$, f_{PV_loss}, α, G_{ref} and T_{c_ref} are the rated DC peak power of the PV generator (W), the efficiency factor (accounting for soiling, wiring losses, etc.), the power temperature coefficient (%/°C) and the standard conditions (1000 W/m^2 and 25 °C), respectively.

The cell temperature is estimated using Equation (26):

$$T_c(t) = T_a(t) + \frac{NOCT - 20}{800} G(t) \quad (26)$$

where $T_a(t)$ is the ambient temperature (°C) and $NOCT$ (°C) is the nominal operation cell temperature. The constants 800 W/m^2 and 20 °C represent the reference irradiance and reference ambient temperature, respectively, specified in standard NOCT test procedures (IEC 61215).

It should be noted that the PV generation profiles are calculated using a physical modeling framework driven by measured 1 min meteorological inputs (irradiance and ambient temperature), rather than empirical generation time series from an operating plant. To ensure realistic power output profiles for the economic assessment, the model explicitly accounts for temperature-dependent efficiency losses, inverter power capacity limits (DC/AC clipping), and overall system derating factors (such as wiring, soiling, and conversion losses).

2.6.2. Wind Turbines Performance

The standard output power curve as a function of wind speed at hub height is supplied by the manufacturer under standard conditions (air density ρ_0 = 1.225 kg/m^3). At each time step t, the standard power curve (Figure 6, green line) is converted to the actual air density power curve (Figure 6, dashed line) by multiplying by the ratio $\rho(t)/\rho_0$, where $\rho(t)$ (kg/m^3) is the actual air density [31].

$$\rho(t) = 3.4837 \frac{p(t)}{T_a(t) + 273.15} \quad (27)$$

where $p(t)$ is the atmospheric pressure (kPa).

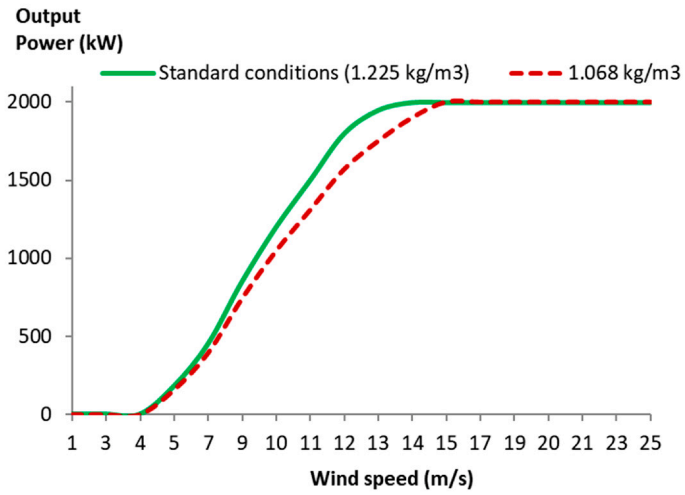


Figure 6. Output power curve of a 2 MW wind turbine with pitch control under standard air density conditions (green) and at a different air density (dashed red).

This time-dependent density value is then directly applied to adjust the wind turbine power curve shown in Figure 6, ensuring precise hourly power output calculations under local atmospheric conditions.

The hub wind speed $v(t)$ (m/s) at hub height z_{hub} (m) is obtained from the measured wind speed $v_{measured}(t)$ at measurement heigh $z_{measured}$ (m), accounting for the terrain roughness length z_0 (m) [31], assuming neutral atmospheric stability conditions:

$$v(t) = v_{measured}(t) \frac{ln\left(\frac{z_{hub}}{z_0}\right)}{ln\left(\frac{z_{measured}}{z_0}\right)} \tag{28}$$

The wind turbine output power $P_{WT_curve}(t)$ is obtained from the real air density power curve. The actual output power, accounting for the turbine inertia effect, is given by Equation (29) [15]:

$$P_{WT}(t) = P_{WT}(t - \Delta t) + (P_{WT_curve}(t) - P_{WT}(t - \Delta t)) \cdot \left(1 - e^{-\Delta t_s \cdot / \tau(t)}\right) \tag{29}$$

where Δt_s is the time step measured in seconds and τ (t) (s) denotes the turbine time constant in seconds (Equation (30)):

$$\tau\ (t) = \tau_0 \frac{v_{rated}}{v(t)} \tag{30}$$

where τ_0 (s) and v_{rated} are the rated time constant and rated wind speed, respectively.

2.6.3. Battery Performance and Degradation Model

This work considers lithium iron phosphate (LFP) batteries—the most prevalent chemistry for stationary energy storage [32]—limiting their C-rate to 2 C to avoid thermal stress and accelerated degradation. To accommodate high-power requirements, lithium titanate oxide (LTO) batteries are also evaluated.

The battery capacity depends on temperature through a polynomial relationship [33] (Equation (31)):

$$C(t) = C_B \cdot (a + b \cdot T(t) + c \cdot T(t)^2) \tag{31}$$

where $T(t)$ (°C) is the battery temperature.

Under PRRC, the battery charge and discharge power are limited by the inverter–charger rated power ($P_{I/Ch}$), the maximum charge/discharge power ($P_{B_C_max}$, $P_{B_D_max}$), and the SOC (Equations (32) and (33)):

$$P_B(t) = min\left(P_B(t),\ P_{I/Ch}, P_{B_C_max}, \frac{C_B(t) \cdot (SOC_{max} - SOC(t))}{100 \cdot \Delta t_h \cdot \eta_{B_C}}\right) \quad \forall P_B(t) > 0\ (charge) \tag{32}$$

$$|P_B(t)| = min\left(|P_B(t)|,\ P_{I/Ch}, P_{B_D_max}, \frac{C_B(t) \cdot (SOC(t) - SOC_{min}) \cdot \eta_{B_D}}{100 \cdot \Delta t_h}\right) \quad \forall P_B(t) < 0\ (discharge) \tag{33}$$

where $SOC(t)$ (%) is the SOC at the beginning of time step t, and η_{B_C} and η_{B_D} are the charge and discharge efficiencies, respectively.

The SOC at the next time step is obtained from Equations (34) and (35):

$$SOC(t + \Delta t) = SOC(t) + \frac{100 \cdot P_B(t) \cdot \eta_{B_C} \cdot \Delta t_h}{C_B} \quad \forall P_B(t) > 0\ (charge) \tag{34}$$

$$SOC(t+\Delta t) = SOC(t) + \frac{100 \cdot P_B(t) \cdot \Delta t_h}{C_B \cdot \eta_{B_D}} \quad \forall P_B(t) < 0 \ (discharge) \tag{35}$$

Degradation Model

Accurate battery degradation estimation is critical for economic calculations, as it determines the number of battery replacements over the system lifetime, affecting the NPV and LCOE.

(a) LFP battery

Cycling degradation is modeled using the Rainflow Counting Algorithm [34], which counts the number of cycles N_m performed annually within each depth of discharge (DOD) range δ_m, over M discrete intervals. The annual capacity loss due to cycling is calculated using Equation (36):

$$C_{loss_cyc}(\%) = C_{loss_EOL}(\%) \sum_{m=1}^{M} \frac{N_m}{CF_m} \tag{36}$$

where CF_m is the number of cycles to failure at DOD range δ_m until the end of life (EOL), defined when capacity loss reaches $C_{loss_EOL}(\%)$ (typically 20%).

CF_m depends on temperature and C-rate [35,36], as shown in Equation (37):

$$CF_m = CF_{m_std} \cdot \frac{\left(\alpha_0 + \alpha_1 \cdot T_{av} + \alpha_2 \cdot {T_{av}}^2\right)}{{C_{rate_av}}^k} \tag{37}$$

where CF_{m_std} is the cycles to failure at 1C and 20 °C (from the manufacturer's DOD curve); T_{av} (°C) is the average battery room temperature; α_0, α_1 and α_2 are fit coefficients (1.7735, −0.0386 and 0.0002 for a commercial LFP battery [37]); C_{rate_av} is the average discharge C-rate; and k is a fit coefficient.

The cycles to failure vs. DOD curve is modeled as a power law [15,38].

$$CF_{m_std} = A_{cyc} \cdot \Delta_m^{B_{cyc}} \tag{38}$$

For a commercial LFP battery [39] at 1C and 20 °C, the fit yields A_{cyc} = 3262 and B_{cyc} = −2.297 (R^2 = 0.9897), with C-rate coefficient k = 0.4838 (Figure 7).

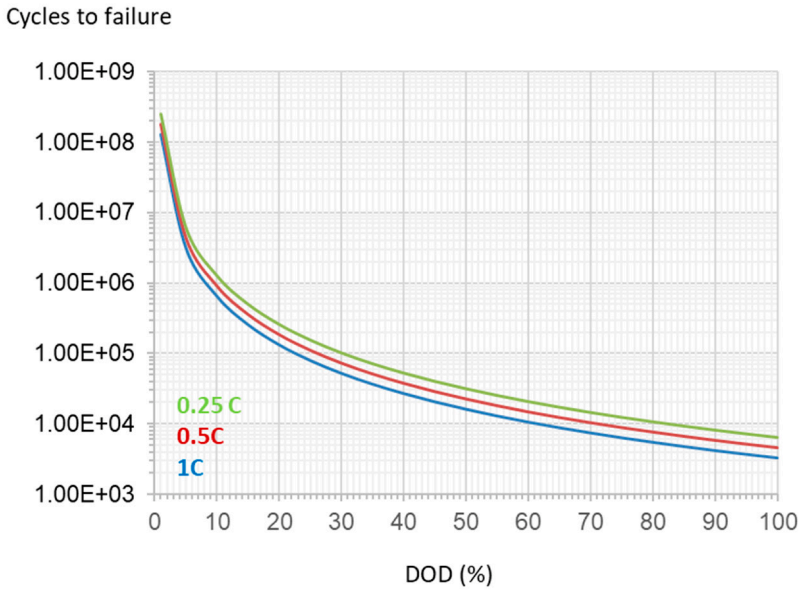


Figure 7. Cycles to failure vs. DOD for a commercial LFP battery at different C-rates (0.25 C, 0.5 C, and 1 C) and temperature of 20 °C [39].

Figure 7 shows the battery cycle-life curves as a function of DOD derived across different discharge C-rates (0.25 C, 0.5 C, and 1.0 C) at a constant operational temperature of 20 °C, using the manufacturer's baseline data (1.0 C at 20 °C) as the reference.

The annual calendar degradation depends on the temperature, time, and SOC [40] (Equation (39)):

$$C_{loss_deg}(\%) = \sum_{j=1}^{J} B_j \cdot e^{-A_j/(RT_j)} \cdot {t_j}^{z_j} \quad (39)$$

where B_j, A_j and z_j [40] are coefficients for each SOC interval j; T_j (K) is the average temperature; and t_j (s) is the annual time spent in that interval.

The battery lifetime LT (years) is estimated by combining cycling and calendar degradation:

$$LT = \frac{C_{loss_EOL}(\%)}{C_{loss_cyc}(\%) + C_{loss_deg}(\%)} \quad (40)$$

subject to $LT \leq LT_{max}$ (15 years assumed for LFP [41]).

(b) LTO battery

The number of full equivalent full cycles to failure (CF_{EFC}) due to cycling degradation is modeled in Equation (41) [42].

$$CF_{EFC} = 32.4 \cdot e^{2196/(273.15+T_{av})} \cdot {C_{rate_av}}^{-0.586} \quad (41)$$

The annual capacity fade due to cycling degradation is calculated using Equation (42):

$$C_{loss_cyc}(\%) = C_{loss_EOL}(\%) \frac{N_{EFC}}{CF_{EFC}} \quad (42)$$

where N_{EFC} is the number of equivalent full cycles performed annually.

Regarding calendar degradation, the capacity loss is low when high SOC levels are avoided and temperatures remain below 45 °C [43,44]. Equation (43) models the annual capacity fade resulting from calendar aging, based on data adapted from Dubarry et al. [43].

$$C_{loss_cyc}(\%) = 1.024 \times 10^{-4} \cdot e^{0.1309 \cdot T_{av}} \cdot (100 - SOC_{av}) \quad (43)$$

where SOC_{av} (%) is the average SOC.

Finally, the service life of LTO batteries is estimated using Equation (40), assuming a maximum operating lifespan of LT_{max}= 25 years [45].

3. Results and Discussion

This section presents the main findings of the study. Section 3.1 details the validation of the proposed model, while Section 3.2 demonstrates its practical application to a case study in Spain.

3.1. Validation of the Proposed Model

The model was validated against the results of Frate et al. [15] for a 200 kW wind turbine located in Costa Rica, considering different inverter–charger power and battery capacity configurations for PRRC. The wind speed and temperature data were obtained from the NSRDB database [46] in 10 min time steps, scaled to a mean wind speed of 6.1 m/s at 50 m hub height [15], with a turbulence intensity of 0.2. The cycling degradation parameters used in [15] were A_{cyc} = 1000, B_{cyc} = −1.5, with no C-rate dependence. Table 1 compares the abatement ratio (AR), storage annuity cost (ACS only for storage), and battery lifetime (LT) (the latter not reported in [15]). The results show good agreement, considering that the original wind speed dataset was not available.

Table 1. Comparison with the results of Frate et al. [15].

Data			Results			
Ramp-Rate Limit (%/min)	**C_B (kWh)**	**T_B(h)**		**Abatement Ratio *AR* (%)**	**Storage Annuity Cost (in kEUR)**	**Battery Lifetime *LT* (yr): A_{cyc} = 1000; B_{cyc} = −1.5 [15]**
5	65	1	Frate et al. [15]	~85	~22	
			This work	88.3	17	5.64
5	65	0.5	Frate et al. [15]	~98	~27	
			This work	99.5	22	4.84
7.5	65	1	Frate et al. [15]	~82	~19	
			This work	87.1	15	6.67
7.5	65	0.5	Frate et al. [15]	~96	~25	
			This work	99.4	21	5.61

The model was also validated against Makibar et al. [27] for a 7.2 MW PV system in Spain with battery-based PRRC under the Puerto Rico penalty system, where the key metric is exported energy ($EE_{\%}$), without economic calculations. Table 2 compares the selected cases, showing good agreement for the $EE_{\%}$. For the battery lifetime—not reported in [27]—two cycling degradation models are considered: the commercial LFP battery in Figure 7 [39] and the model used by Frate et al. [15], both with k = 0.4838 [39] and assuming a constant temperature of 20 °C.

Table 2. Comparison with the results of Makibar et al. [27].

Data				Results			
Ramp-Rate Limit (%/min)	**C_B (kWh)**	**$P_{I/Ch}$ (kW)**	***C* − *rate***		**Exported Energy $EE_{\%}$ (%)**	**Battery Lifetime *LT* (yr)**	
						A_{cyc} = 3262; B_{cyc} = −2.297 Figure 7 [39]	A_{cyc} = 1000; B_{cyc} = −1.5 [15]
10	874	5148	5.9C	Makibar [27]	100		
				This work	100	22.24	10.49
10	254	1493	5.9C	Makibar [27]	100		
				This work	100	12.86	2.94
10	328	1313	4C	Makibar [27]	100		
				This work	100	16.43	4.26
10	874	514.8	0.59C	Makibar [27]	80		
				This work	83	23.48	19.26
10	87.4	514.8	5.9C	Makibar [27]	80		
				This work	83	12.79	2.88
10	184	1081	5.9C	Makibar [27]	97		
				This work	98.4	11.29	2.25
10	572	1030	1.8C	Makibar [27]	97		
				This work	98	22.29	9.44

3.2. Case Study in Spain

A case study located in El Perdón, Navarra (Spain) is considered.

The monthly irradiance statistics and wind speed data are shown in Figures 8–10. Figure 8 illustrates the monthly mean horizontal irradiance along with its seasonal variability (±1 standard deviation, min/max).

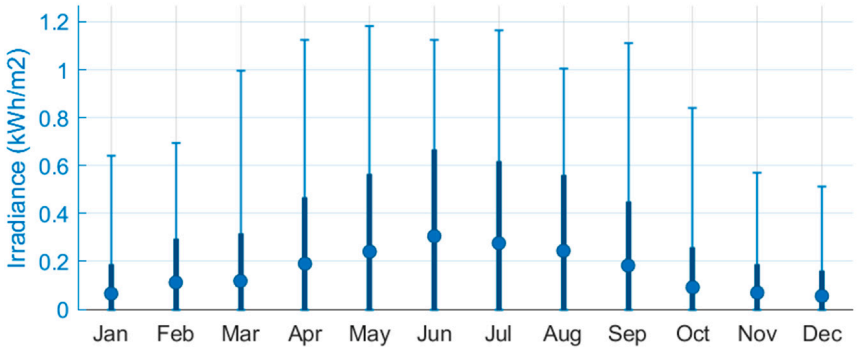


Figure 8. Horizontal irradiance: monthly mean, ±1 standard deviation, and minimum/maximum values.

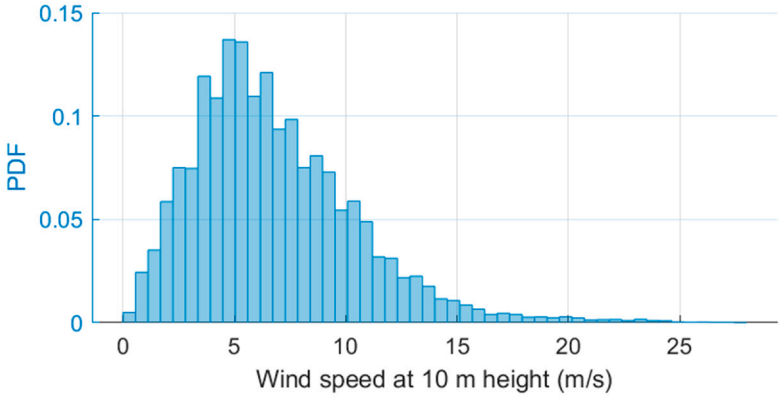


Figure 9. Wind speed at 10 m height: probability density histogram (annual mean: 6.83 m/s).

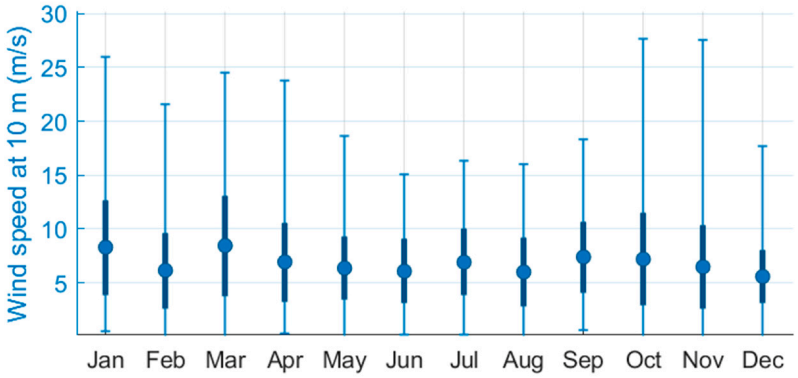


Figure 10. Wind speed at 10 m height: monthly mean, ±1 standard deviation, and minimum/maximum values.

The meteorological data—comprising irradiance on a horizontal surface, wind speed at a 10 m height, and ambient temperature—consist of real measurements for the year 2025 downloaded from the Government of Navarra [47] in 10 min time steps. One-minute time-step irradiance data were obtained using a first-order autoregressive function [26] with a standard deviation of 0.15 [48] and a correlation coefficient of 0.5. These horizontal data were then converted to a 40° slope utilizing the Hay, Davies, Klucher, and Reindl model [49]. Similarly, the 10 m wind speed was converted to 1 min steps by considering a turbulence intensity of 0.12 [47] and a correlation of 0.5; it was subsequently extrapolated to a 100 m hub height using a roughness length of 0.1 m.

The annual inclined solar irradiation is 1579 kWh/m^2 per year (40° tilt, south facing), corresponding to an annual average of 4.33 equivalent peak sun hours (PSH) per day (1579 peak hours per year).

The selected site possesses an excellent wind resource characterized by an annual mean wind speed of 6.83 m/s at the 10 m reference height, which supports operational commercial wind farms in the immediate region.

Both LFP and LTO battery technologies are evaluated in this analysis. A C-rate limit of 2 C is established for LFP batteries, whereas LTO batteries are constrained to a maximum C-rate of 6 C. For both chemistries, the minimum and maximum SOC limits are set to 10% and 90%, respectively. The auxiliary load of the battery system (cooling, heating, instrumentation, control, and lighting) is 1.8 kW per MWh of nominal capacity [50]. The POI maximum power is 6 MW and the ramp-rate limit is 10%/min.

The nominal power of each system configuration and the annual exported energy without ramp-rate limitation are summarized in Table 3.

Table 3. Nominal power and exported energy without ramp-rate limitation for each system configuration.

	PV System	**Wind System**	**PV–Wind System**
Nominal power	6 MW_ac (7.5 MW_dc)	6 MW (3 turbines of 2 MW)	PV: 2 MW_ac PV (2.5 MW_dc) Wind: 6 MW
POI maximum power (MW)	6	6	6
EE (GWh/yr)	8.896	25.279	27.848

All technical specifications, efficiency metrics, degradation rates, and unit cost breakdowns (including installation CAPEX and O&M) for the PV, wind turbines, power converters, and energy storage systems are systematically summarized in Table 4.

Table 4. System parameters.

Variable	**Value**
Location	42.733° N, 1.715° W
Height above sea level	1024 m
Meteorological data	Navarra government [47], year 2025
Annual irradiation (40° tilt, south facing)	1579 kWh/m^2
Average wind speed, $z_{measured}$ = 10 m	6.83 m/s
Wind speed Weibull factor	2.1
Average ambient temperature	12.38 °C
POI max. grid power P_{max_grid}	6 MW
Hourly electricity price	Two cases: (a) Spot market, 2025 in Spain; (b) hypothetical stretched curve (Figures 11 and 12)
Hourly electricity price: average, standard deviation, minimum and maximum	65.3, 47.6, −15, 240 EUR/MWh 102.9, 101.1, −7.5, 480 EUR/MWh
Daily electricity price spreads: average, standard deviation, minimum and maximum	98.1, 35.9, 12.1, 209.3 EUR/MWh 232.1, 77.7, 18.2, 429.8 EUR/MWh
Annual electricity price escalation rate Inf_{Pr}	2%
PV:	
$CAPEX_{PV}$	0.7 EUR/Wac [51]
$OPEX_{PV}$	1% of CAPEX per year [51]

Table 4. *Cont.*

Variable	Value
Slope and azimuth	40° and 0° (south facing)
Lifetime	20 years
NOCT	43 °C
f_{PV_loss}	95%
α	−0.4%/°C
Inverter efficiency	Variable, max. 96% [26]
Wind:	
$CAPEX_W$	1.4 EUR/W (Ref. [51])
$OPEX_W$	2% of CAPEX per year [51]
Lifetime	20 years
Hub height z_{hub}	100 m
Roughness length z_0	0.1 m
Power curve	Figure 6
Time constant τ_0	22 s [15]
Battery:	
$CAPEX_B$	LFP: 75 EUR/kWh [52]; LTO: 300 EUR/kWh [53]
Cost escalation (for replacements)	−3.5% (Ref. [54])
$OPEX_B$	2% of CAPEX per year (Ref. [54])
Max. power $P_{B_C_max} = P_{B_D_max}$	LFP: $2 \cdot C_N$/h; LTO: $6 \cdot C_N$/h (MW)
Roundtrip efficiency	90%
Auxiliary electrical consumption	1.8 kW per MWh of nominal capacity [50]
Cycle life	LFP: Figure 7; LTO: Equation (41)
Battery inverter–charger:	
$CAPEX_{I/Ch}$	100 EUR/kW [52,54]
Cost escalation (for replacements)	2% (general inflation)
$OPEX_{I/Ch}$	0% (included in battery)
Lifetime	10 years
Efficiency	Variable, max. 96% [26]

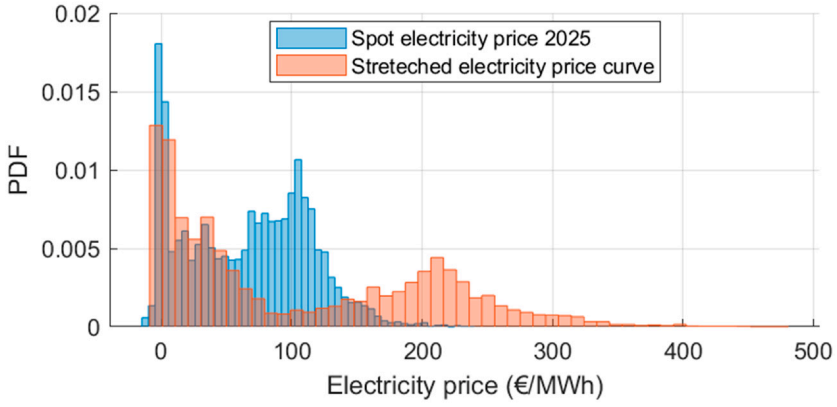


Figure 11. Probability density histogram of Spain's 2025 spot electricity price and the stretched curve.

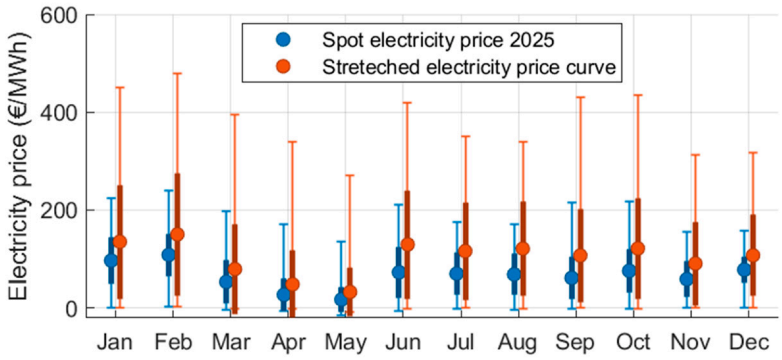


Figure 12. Monthly mean, ±1 standard deviation, and minimum/maximum values of Spain's 2025 spot electricity price and the stretched curve.

Two penalty systems (Section 2.2) are considered:

- Limiting maximum POI power penalty system (as in Puerto Rico) [27].
- Fee penalty system with a fee of 4668.59 EUR/MWh [30].
- Two electricity price scenarios are also considered (Figures 11 and 12):
- Spot hourly electricity market price for Spain in 2025.
- Hypothetical stretched price curve: peaks multiplied by two and valleys divided by two.

The system parameters are listed in Table 4. The system lifetime is 20 years, interest rate is 8% and general inflation is 2%.

It should be noted that the quantitative results presented in this study are based on a single-year dataset (2025). While absolute economic outcomes (such as specific net profits or optimal battery capacities) are subject to inter-annual weather variability and market price fluctuations, the primary objective of this work is methodological and comparative. The proposed decision tree logic, the dynamic degradation formulation, and the relative economic rankings between non-storage PRRC strategies and dual-use battery storage provide a generalizable framework that remains applicable across different years and regional market structures.

For each system type under the battery-based scenarios, joint optimization of the battery storage and inverter–charger sizing for PRRC—including state-of-charge (SOC) operating limits and price thresholds where arbitrage is considered—was conducted separately for LFP and LTO battery chemistries. Table 5 summarizes the optimization variables, including their operational ranges and step sizes.

Table 5. Ranges and resolutions of optimization variables for battery-based PRRC scenarios.

Optimization Variable	Unit	Range	Step Size
Battery nominal capacity C_B	MWh	0.1–2.0	0.1
Inverter/charger rated power $P_{I/Ch}$	MW	0.1–4.0	0.1
Arbitrage control variables:			
SOC limits (SOC_{A_min}, SOC_{A_max})	%	10–90	10
Price thresholds ($Pr_{A_High_C}$, $Pr_{A_Low_D}$)	EUR/MWh	0–150	30

Exhaustive optimization of systems with arbitrage, covering all parameter combinations, would require approximately 97 h (583,200 cases on an Intel Core i5-6500 at 3.2 GHz with 16 GB RAM, at 0.6 s/case). The Genetic Algorithm (GA) optimization was completed in 0.43 h, yielding strong performance, as detailed in Section 3.2.2. The GA parameters were adapted from effective configurations identified in prior renewable system optimization work [55]: 15 generations, a crossover rate of 90%, and a mutation rate of 1%. However,

the population size was increased to 0.03% of the search space—ten times higher than the 0.003% recommended in [55]. This adjustment was necessary because the search space in this study is significantly smaller; adhering strictly to 0.003% yielded only 17 individuals, an overly small population that led to degraded optimization convergence.

3.2.1. Results for Spot Electricity Price in Spain in 2025

Table 6 shows the results of the optimal battery and inverter–charger for the battery PRRC scenarios (with curtailment; only used when the battery cannot eliminate the ramp-up violation) without arbitrage. Because all optimized scenarios demand operational C-rates reaching or exceeding 2, LTO battery chemistry is indispensable to accommodate the required high-power charge and discharge dynamics. Under the limiting POI power penalty system (Puerto Rico), the optimal battery capacity is the minimum considered (0.1 MWh), with a C-rate of 2–4 in all cases, since only a sufficient weekly RRC is needed to avoid POI power curtailment the following week. Under the fee penalty system, both the optimal battery capacity and C-rate are higher (5–6), as greater inverter–charger power is required to reduce non-compliant energy and thus minimize penalty costs.

Table 6. Results of the optimal systems for the battery PRRC scenarios without arbitrage.

	PV System		**Wind System**		**PV–Wind System**	
Penalty System	**Limiting POI**	**Fee**	**Limiting POI**	**Fee**	**Limiting POI**	**Fee**
C_B (MWh)	0.1	0.2	0.1	0.6	0.1	0.3
Battery type	LTO	LTO	LTO	LTO	LTO	LTO
$P_{I/Ch}$ (MW)	0.4	1.2	0.2	3	0.4	1.5
T_B (h)	0.25	0.166	0.5	0.2	0.25	0.2
C_rate	4	6	2	5	4	5
EE (MWh/yr)	8762	8842	25,161	25,221	27,756	27,768
Charge energy (MWh/yr)	62	92	24	61	32	45
Discharge energy (MWh/yr)	57	84	22	55	29	41
LT (yr)	31.88	42.73	84.95	193.1	61.7	128.8
No. of violations	3658	481	2458	149	878	173
RRC	99.30	99.91	99.53	99.97	99.83	99.97
AR	70.95	98.32	82.54	99.36	93.18	99.25
Battery lifetime: min(LT,LT_{max}) (yr)	25	25	25	25	25	25

Across all cases, the battery charge and discharge energy throughput is negligible compared to the total exported energy *EE*. Furthermore, because the calculated battery lifetime significantly exceeds the maximum lifetime constraint LT_{max}, this upper limit is adopted as the final operational lifespan.

Table 7 shows the optimal battery, inverter–charger, and control parameters for the battery PRRC scenarios (with curtailment) with arbitrage. The optimal battery capacity is slightly higher than in the cases without arbitrage; however, the charge and discharge energy remain negligible, resulting in no significant NPV improvement, as shown in the following figures. Only in two of the six cases—specifically, the PV system and the wind system with a limiting POI power penalty system—is the C-rate lower than 2, allowing

for the use of LFP batteries. In the remaining four cases, the C-rate is 4 or higher, thereby requiring LTO batteries. For both the PV and wind systems, the SOC operating limits for energy arbitrage range from 20% to 80% (a 60% SOC window). In contrast, the hybrid PV–wind system operates within a narrower arbitrage range (a 40% window). Regarding the price thresholds for arbitrage, the scenarios with POI power-limiting penalties set the upper charging limit to 30 EUR/MWh and the lower discharging limit to 90 EUR/MWh. In the fee penalty scenarios, these thresholds increase to 90 EUR/MWh (60 EUR/MWh for the wind system) for charging and 150 EUR/MWh for discharging.

Table 7. Results of the optimal systems for the battery PRRC scenarios with arbitrage.

	PV System		**Wind System**		**PV–Wind System**	
Penalty System	**Limiting POI**	**Fee**	**Limiting POI**	**Fee**	**Limiting POI**	**Fee**
C_B (MWh)	0.3	0.3	0.6	0.6	0.1	0.3
Battery type	LFP	LTO	LFP	LTO	LTO	LTO
$P_{I/Ch}$ (MW)	0.4	1.5	0.2	3	0.4	1.5
T_B (h)	0.75	0.2	3	0.2	0.25	0.2
C_rate	1.33	5	0.33	5	4	5
SOC_{A_min} (%)	20	20	20	20	40	30
SOC_{A_max} (%)	80	80	80	80	80	70
$Pr_{A_High_C}$ (EUR/MWh)	30	90	30	60	30	90
$Pr_{A_Low_D}$ (EUR/MWh)	120	150	90	150	90	150
EE (MWh/yr)	8785	8858	25,159	25,222	27,769	27,775
Charge energy (MWh/yr)	86	107	110	67	42	54
Discharge energy (MWh/yr)	78	102	98	61	38	50
No. of violations	3782	214	2677	179	1452	244
RRC	99.28	99.96	99.49	99.97	99.72	99.95
AR	69.97	99.25	8.98	99.24	88.72	98.95
LT (yr)	18.69	44.51	19.72	142.31	39.92	95.43
Battery lifetime: min(*LT*,LT_{max}) (yr)	15	25	15	25	25	25

The results for the different scenarios are shown in Figure 13 (PV), Figure 14 (wind), and Figure 15 (PV–wind). The blue bars correspond to the limiting POI power penalty system and the orange bars to the fee penalty system. "No RR limit" denotes the scenario without ramp-rate limitation (unconstrained case), which is included for reference. The analyzed scenarios are defined as follows: 'No PRRC' represents the no ramp-rate control scenario; 'C' denotes the curtailment scenario; 'R10%' corresponds to the scenario with a 10% power reserve for renewable generation; and 'C+R10%' combines curtailment with a 10% power reserve. Additionally, 'B+C' refers to the scenario with an optimal battery dedicated solely to PRRC and curtailment, where curtailment is only utilized when the battery cannot mitigate the ramp-up violation. Finally, 'B(A)+C' represents the scenario incorporating an optimal battery for PRRC and arbitrage, supplemented by curtailment.

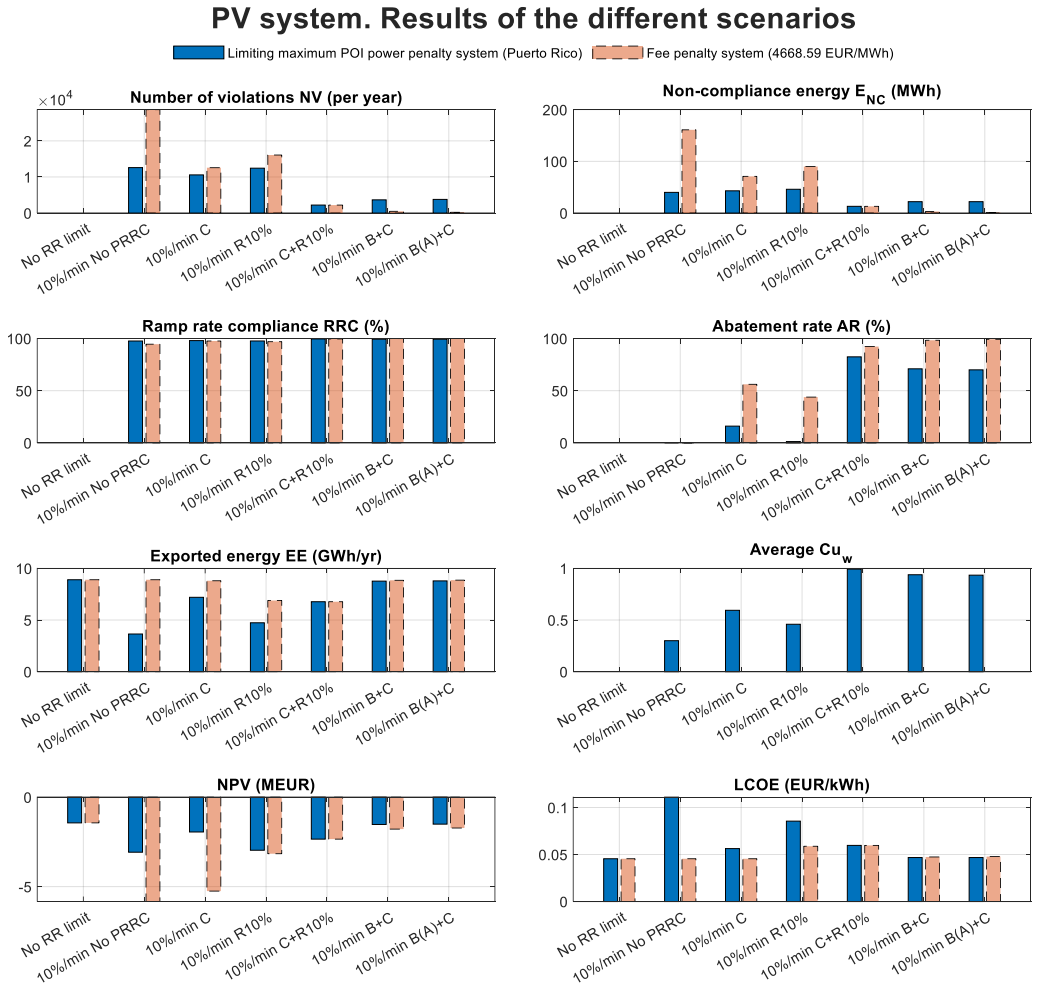


Figure 13. Spain's 2025 spot electricity price. Results for the PV system with 10%/min ramp-rate limits. Blue bars: Limiting maximum POI power penalty system (Puerto Rico); orange bars: fee penalty system (4668.59 EUR/MWh). Scenario labels—No RR limit: no ramp-rate limitation (unconstrained case); No PRRC: no ramp-rate control; C: curtailment; R10%: 10% power reserve; C+R10%: curtailment and 10% power reserve; B+C: optimal battery and curtailment (curtailment is only used when the battery cannot eliminate the ramp-up violation); B(A)+C: optimal battery with arbitrage and curtailment.

Note that even without ramp-rate limitation, the PV system NPV is negative, as the Spain spot price curve for 2025 includes many hours at or near zero EUR/MWh at noon.

Figures 13–15 show that, across the three system configurations, the number of violations in the "no PRRC" scenario exceeds 10,000 under the POI power-limiting penalty scheme and 20,000 under the fee penalty system. This marked disparity arises because the curtailment factor in the POI power-limiting scheme decreases over successive weeks; as a result, the POI power output is reduced, lowering the frequency of violations—albeit at the expense of total energy injected into the grid. Relying solely on curtailment or solely on a 10% power reserve for PRRC fails to yield a significant reduction in violations. Achieving a meaningful reduction requires either combining curtailment with a 10% power reserve or integrating battery storage for PRRC.

For PV systems with a fee penalty system, a 10% power reserve yields better economic results than curtailment alone (higher NPV, lower LCOE), whereas the opposite holds for the other penalty system and for wind and PV–wind systems. The combination of curtailment and 10% power reserve improves the results further. The optimal battery system (with curtailment) achieves *EE*, *NPV*, and *LCOE* values comparable to the no ramp-

rate-limitation case. Adding arbitrage produces negligible *NPV* and *LCOE* improvements. In summary, under ramp-rate limitations, the optimal battery system is the only PRRC strategy that achieves economic performance comparable to the unconstrained case.

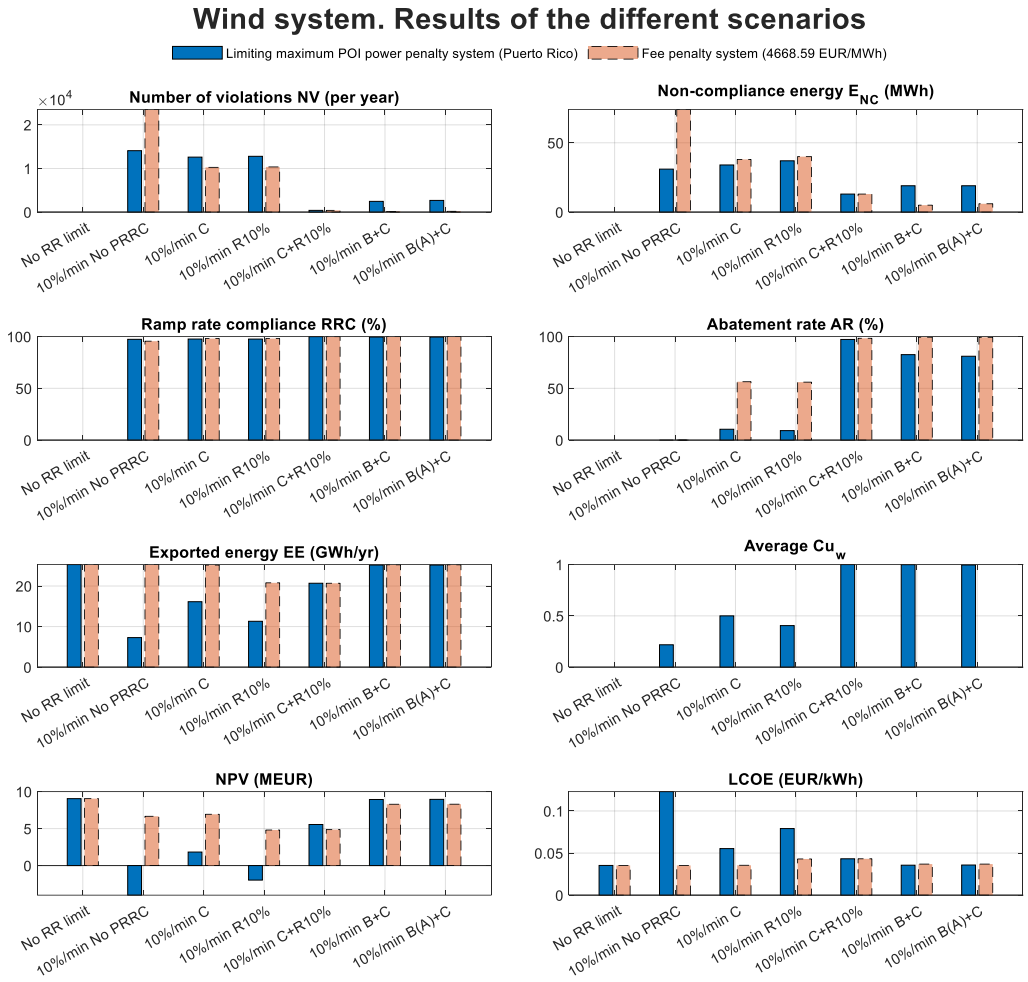


Figure 14. Spain's 2025 spot electricity price. Results for the wind system with 10%/min ramp-rate limits.

Figure 16 shows the weekly curtailment factor for the PV–wind system scenarios. Curtailment combined with a 10% power reserve, or battery-based PRRC, maintains a curtailment factor of one throughout the year.

To illustrate the performance of the different PRRC strategies, Figure 17 shows the simulation of the PV–wind system on 11 January (week 2) under the limiting POI power penalty system. Each subplot includes two insets: one for 0:50–1:10 (ramp-up violation at 1:00) and one for 4:10–4:30 (ramp-up violation at 4:20). Without PRRC (a), multiple ramp-rate violations occur. Curtailment (b) eliminates ramp-up violations but not ramp-down violations. A 10% power reserve (c) reduces ramp-down violations. Combined curtailment and power reserve (d) eliminates most violations, except the large ramp-down event at 4:20, which is reduced but not fully eliminated. The optimal 0.1 MWh battery system (e) shows similar residual violations due to the inverter–charger power limit (0.4 MW), but delivers higher output power than (d)—since no power reserve is required—resulting in a significantly higher NPV.

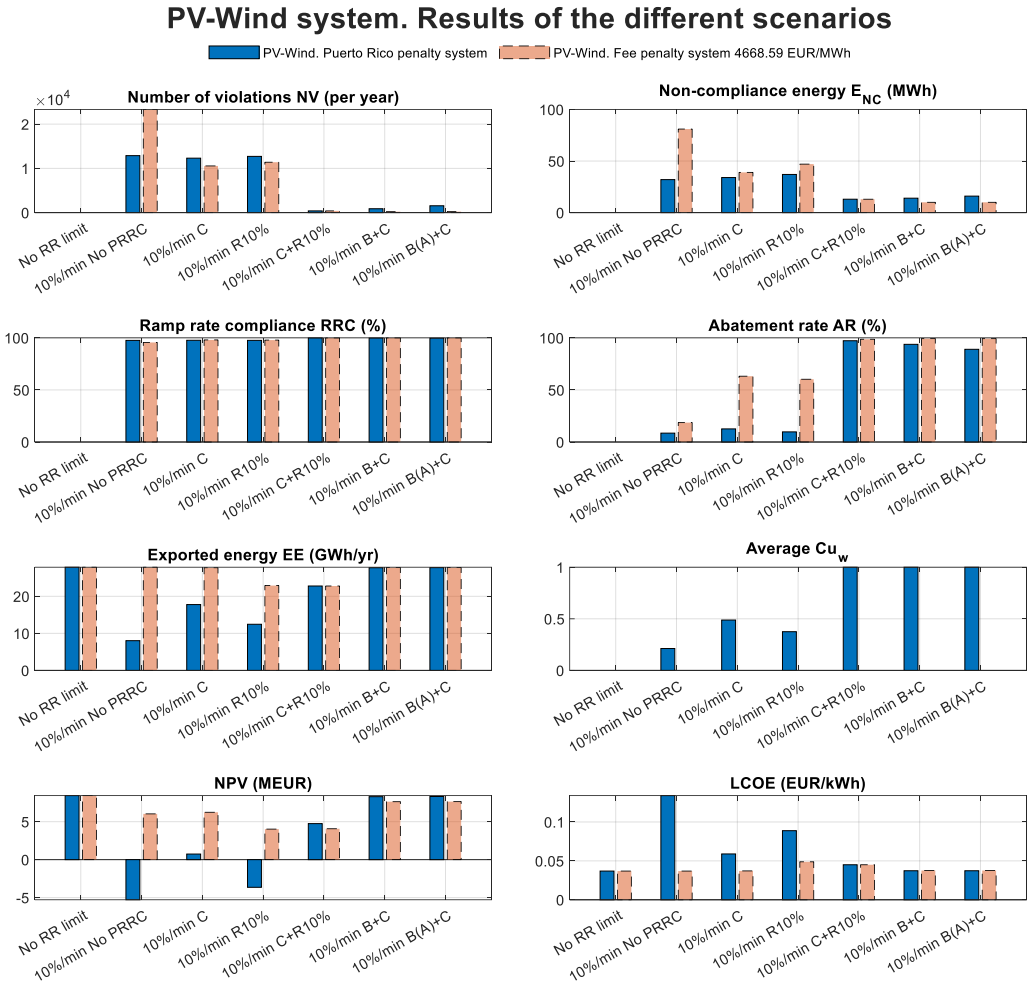


Figure 15. Spain's 2025 spot electricity price. Results for the PV–wind system with 10%/min ramp-rate limits.

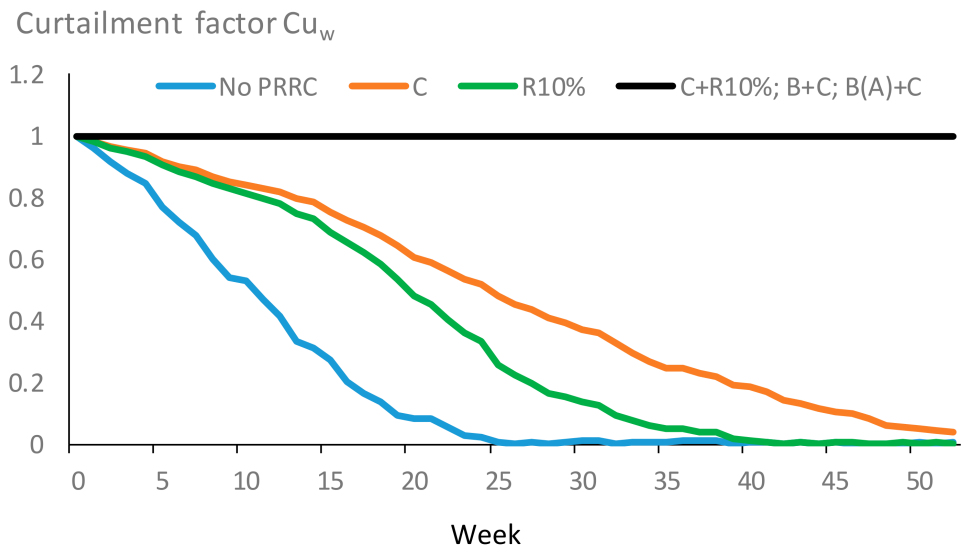


Figure 16. Weekly curtailment factor for the PV–wind system scenarios with 10%/min ramp-rate limits.

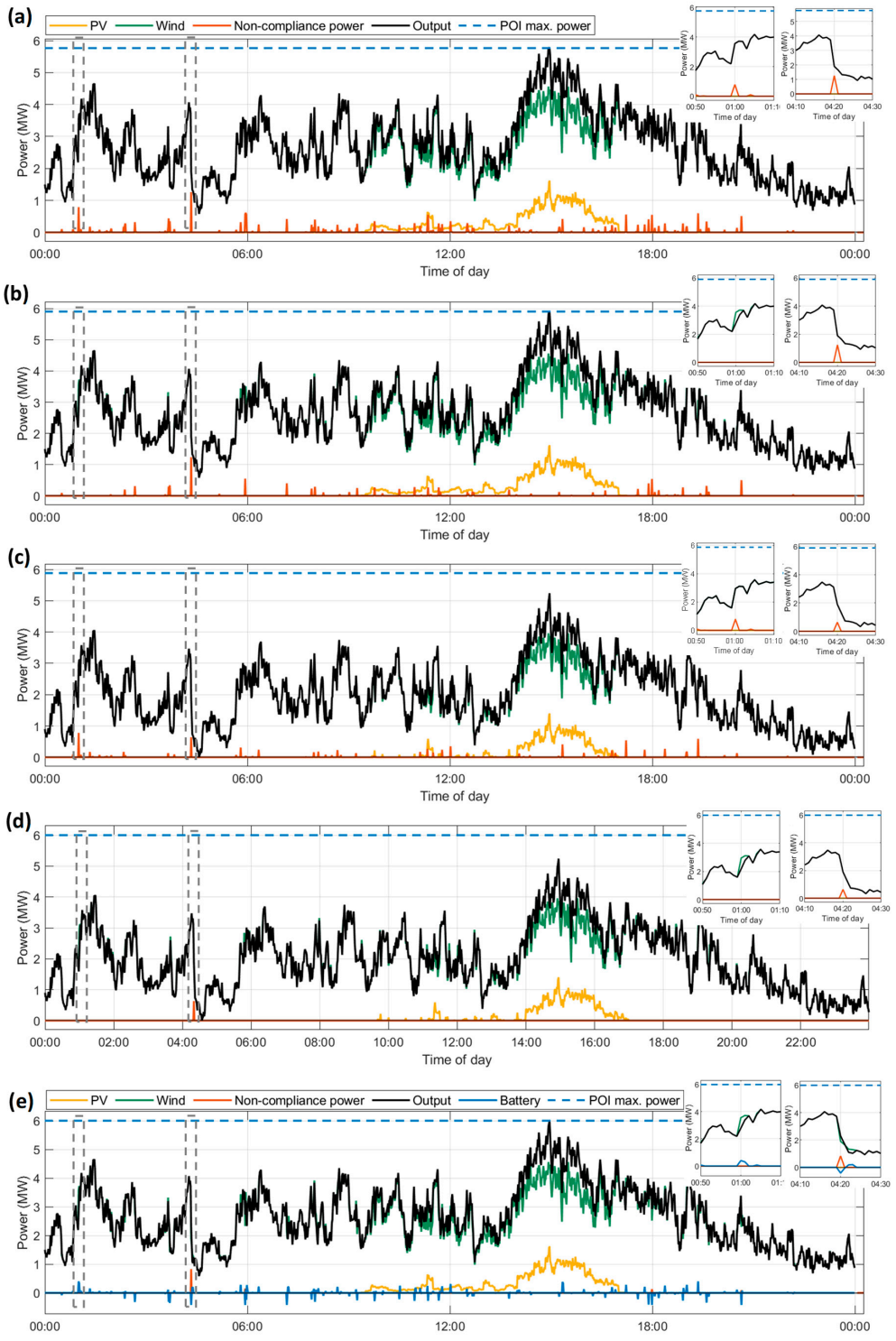


Figure 17. PV–wind system simulation on 11 January: 10%/min ramp-rate limits, limiting maximum POI power penalty system. (**a**) No PRRC, (**b**) curtailment, (**c**) 10% power reserve, (**d**) curtailment and 10% power reserve, (**e**) optimal battery system and curtailment.

3.2.2. Validation of GA Optimization for the 2025 Spanish Electricity Spot Market

For the B(A)+C scenarios (optimal battery with arbitrage and curtailment under a 10%/min ramp-rate limit, considering both the maximum POI power limit penalty and fee penalty systems), exhaustive optimizations covering all parameter combinations were compared against the GA performance. The exhaustive optimization required over 97 h of execution time, whereas the GA required approximately 0.4 h. For each scenario, the GA

was executed 20 times. In most cases, the GA identified the global optimum (matching the exhaustive optimization results).

Two statistical parameters were selected to evaluate the performance and stability of the GA [56]: root mean square error (*RMSE*) and mean efficiency (η). These statistical parameters evaluate performance based on the NPV as the objective function. The results in Table 8 demonstrate the robust performance of the GA.

Table 8. Statistical parameters of the GA for B(A)+C scenarios using 2025 Spanish electricity spot market.

Scenario	**PV B(A)+C**		**Wind B(A)+C**		**PV–Wind B(A)+C**	
Penalty System	**POI**	**Fee**	**POI**	**Fee**	**POI**	**Fee**
Success Count (out of 20)	19	17	18	18	18	17
RMSE (MEUR)	0.0043	0.0082	0.0132	0.0187	0.0171	0.0198
η (%)	99.96	99.92	99.91	99.86	99.87	99.83

3.2.3. Results for Stretched Electricity Price Curve

This section analyzes a hypothetical stretched electricity price curve (Figures 11 and 12) characterized by higher daily price spreads (232.1 EUR/MWh vs. 98.1 EUR/MWh) and a higher average electricity price (102.9 EUR/MWh vs. 65.3 EUR/MWh) compared to the 2025 Spanish market.

The technical outcomes for the optimal system configurations under both non-battery PRRC scenarios and battery PRRC scenarios operating without arbitrage are identical to those reported in Section 3.2.1.

In the arbitrage scenarios, the initial optimization runs reached the maximum battery capacity (2 MWh), so the search space was extended to 50 MWh (and 10 MW for the inverter–charger) (Table 9).

Table 9. Ranges and resolutions of optimization variables for battery-based PRRC scenarios with arbitrage: stretched electricity price curve.

Optimization Variable	**Unit**	**Range**	**Step Size**
Battery nominal capacity C_B	MWh	2–50	2
Inverter/charger rated power $P_{I/Ch}$	MW	1–10	1
Arbitrage control variables:			
State-of-charge limits (SOC_{A_min}, SOC_{A_max})	%	10–90	10
Price thresholds ($Pr_{A_High_C}$, $Pr_{A_Low_D}$)	EUR/MWh	0–210	30

Across all cases, the optimal system configuration utilized LFP battery chemistry, as the peak operational C-rate remained below 0.21 (Table 10). Arbitrage proved worthwhile, with optimal battery capacities of 44, 28, and 40 MWh for the PV, wind, and PV–wind systems, respectively, and an optimal inverter–charger power of 6 MW in all cases. The SOC operating limits for energy arbitrage spanned from 20% to 90% (a 70% SOC window). Regarding the price thresholds for arbitrage, the upper charging limit was set to 90 EUR/MWh for the PV system and 60 EUR/MWh for the remaining configurations, whereas the lower discharging limit was 120 EUR/MWh across all cases.

Arbitrage results in high charge/discharge energy (particularly for the PV system) and eliminates all ramp-rate violations.

Figure 18 shows the results for the PV system. As in Section 3.2.1, the optimal battery is the only PRRC strategy that achieves economic results comparable to the unconstrained case; however, the NPV remains negative. With battery PRRC and arbitrage, the NPV

becomes positive (6 million EUR; due to high revenue from peak-price electricity sales), whereas all other scenarios yield a negative NPV.

Table 10. Optimal battery capacity and inverter–charger power for battery PRRC with arbitrage under the stretched price curve for each system type (results are identical for both penalty systems, as all violations are eliminated).

	PV System	Wind System	PV–Wind System
C_B (MWh)	44	28	40
Battery type	LFP	LFP	LFP
$P_{I/Ch}$ (MW)	6	6	6
T_B (h)	7.33	4.66	6.66
C_rate	0.14	0.21	0.15
SOC_{A_min} (%)	20	20	20
SOC_{A_max} (%)	90	90	90
$Pr_{A_High_C}$ (EUR/MWh)	90	60	60
$Pr_{A_Low_D}$ (EUR/MWh)	120	120	120
EE (MWh/yr)	7410	24,131	26,359
Charge energy (MWh/yr)	6604	4305	5984
Discharge energy (MWh/yr)	5949	3884	5403
LT (yr)	21.14	19.44	19.53
Battery lifetime: min(*LT*,LT_{max}) (yr)	15	15	15

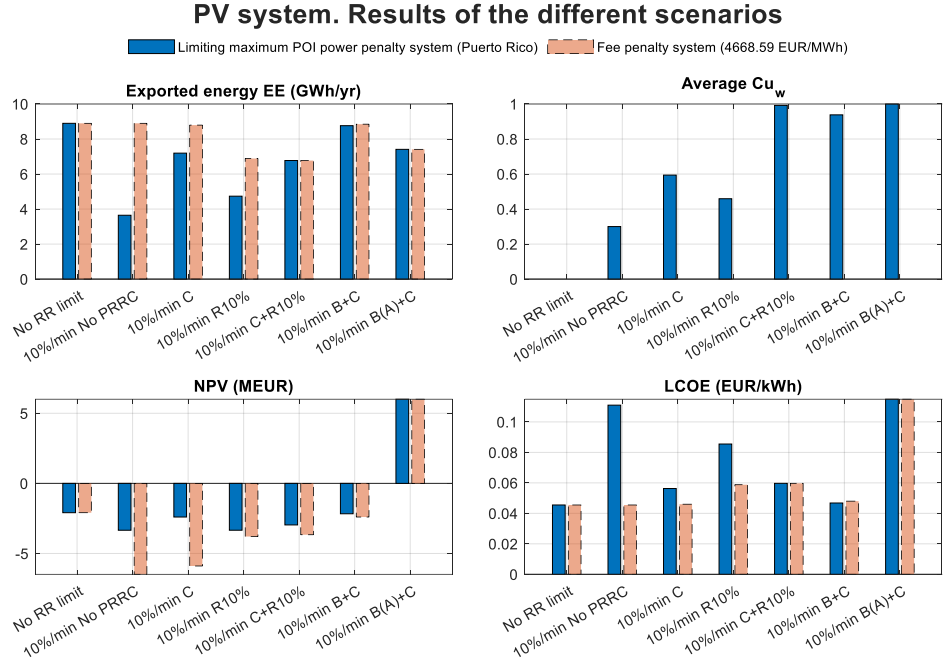


Figure 18. Stretched electricity price curve. Results for the PV system with 10%/min ramp-rate limits.

Figures 19 and 20 show the results for the wind and PV–wind systems, respectively. In both cases, the optimal battery is the only PRRC strategy yielding economic results comparable to the unconstrained case, and adding arbitrage produces a significant NPV increase.

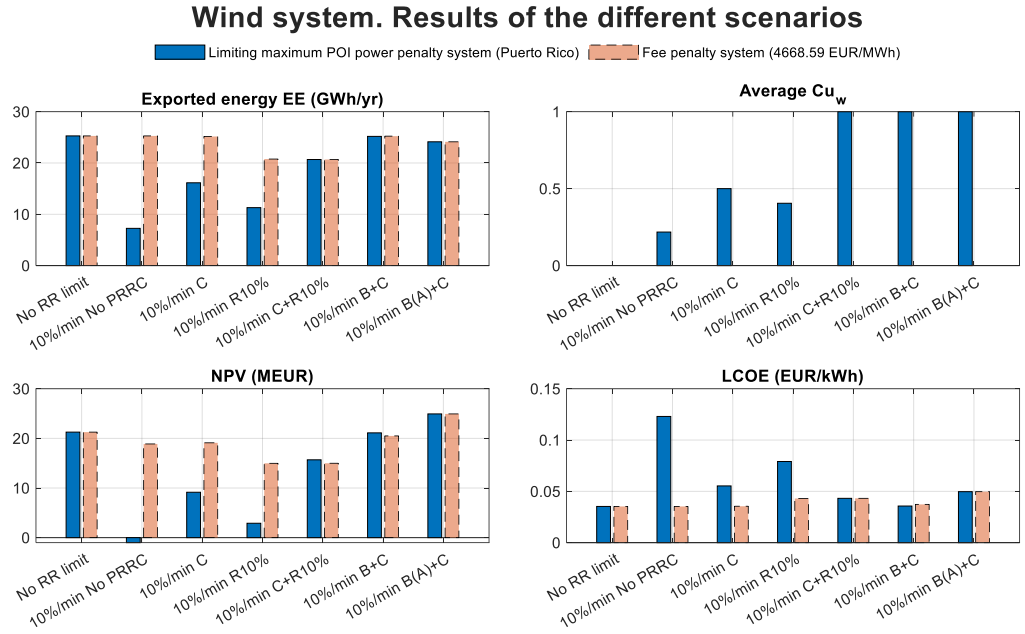


Figure 19. Stretched electricity price curve. Results for the wind system with 10%/min ramp-rate limits.

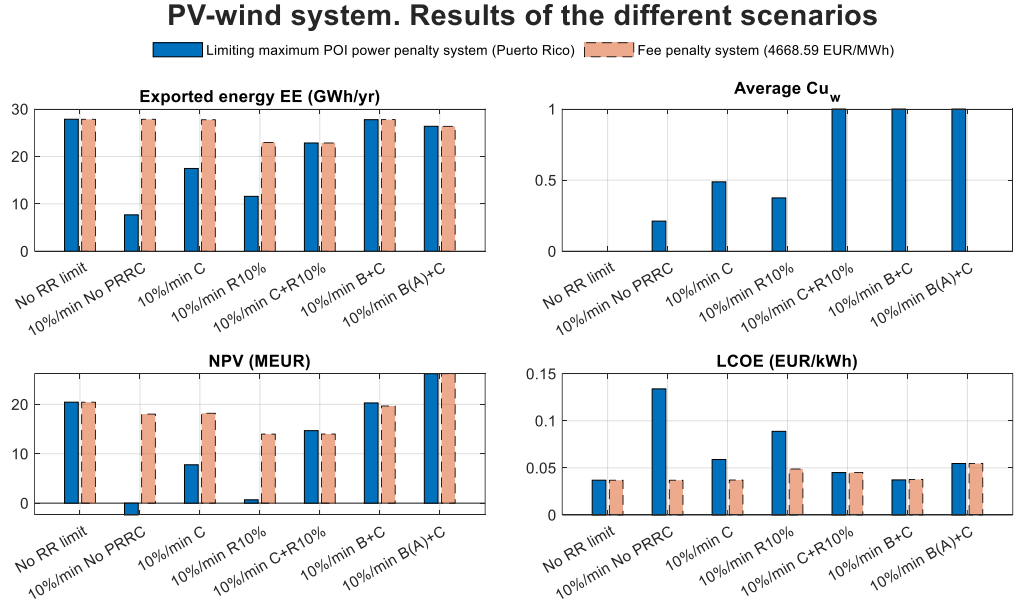


Figure 20. Stretched electricity price curve. Results for the PV–wind system with 10%/min ramp-rate limits.

Figure 21 shows a two-day simulation (11–12 January) of the PV–wind system with the optimal battery for PRRC and arbitrage; the SOC limits shown correspond to the arbitrage SOC bounds. During 0:00–3:00, the electricity price exceeds the discharge threshold, but the battery remains at SOC_{A_min} and only operates briefly to prevent ramp-rate violations. From 3:00 to 8:00, the battery charges (arbitrage) while no power is injected into the grid. From 8:00 to 11:00, the battery discharges (arbitrage), supplementing the renewable output up to the 6 MW POI limit. From 11:00 to 17:00, the battery charges again, and from 17:00 onward it discharges until reaching SOC_{A_min} before 22:00.

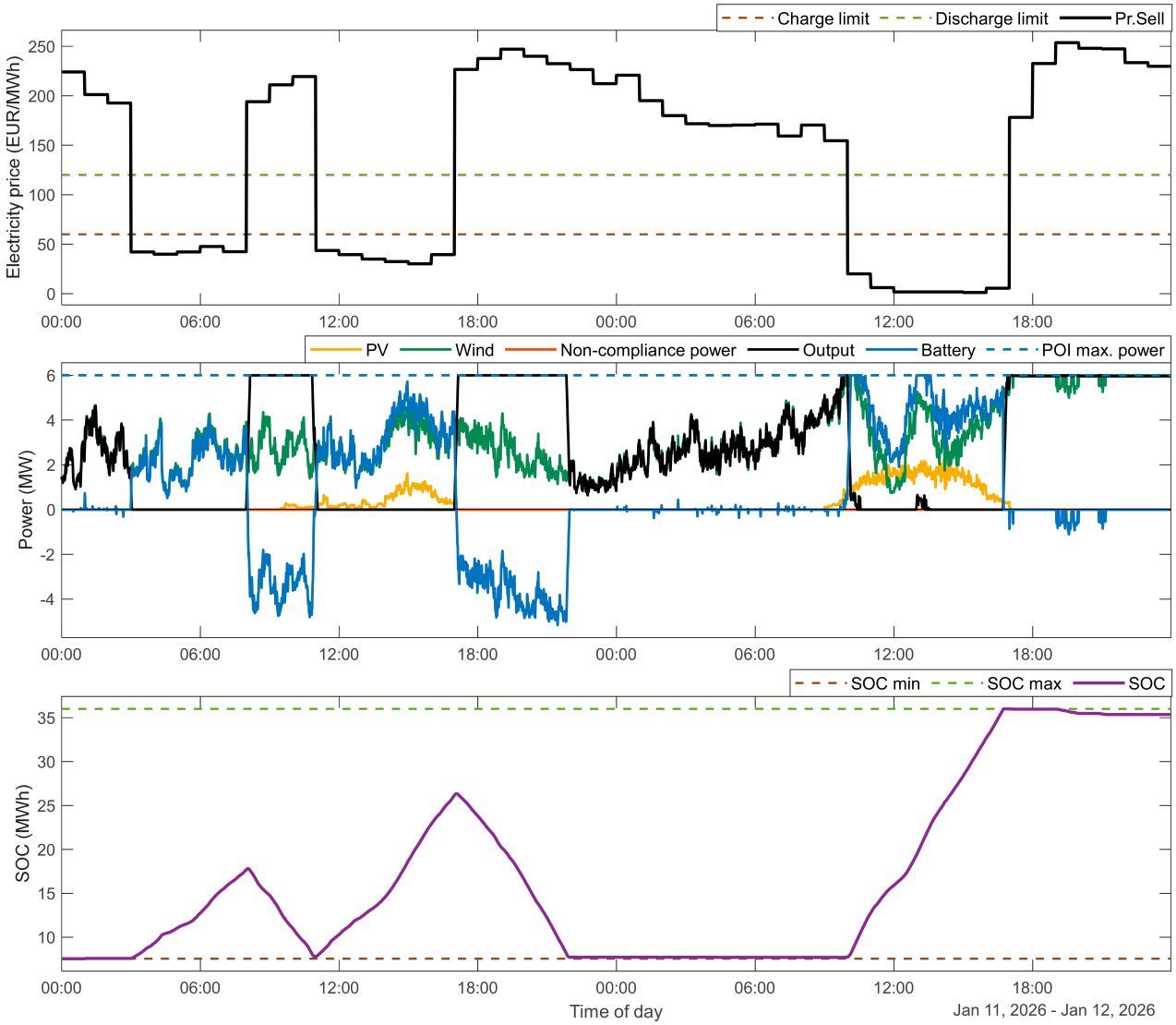


Figure 21. Stretched electricity price curve. Simulation of the PV–wind system with optimal battery for PRRC and arbitrage and 10%/min ramp-rate limits for 11–12 January.

3.2.4. Validation of GA Performance for the Stretched Electricity Price Curve

Table 11 presents the statistical parameters of the Genetic Algorithm (GA) for the B(A)+C scenarios under the stretched electricity price curve. The results demonstrate strong optimization performance, consistent with the findings in Section 3.2.2.

Table 11. Statistical parameters of the GA for the B(A)+C scenarios: stretched electricity price curve.

Scenario	**PV B(A)+C**		**Wind B(A)+C**		**PV–Wind B(A)+C**	
Penalty System	**POI**	**Fee**	**POI**	**Fee**	**POI**	**Fee**
Success Count (out of 20)	18	17	20	17	18	18
RMSE (MEUR)	0.0145	0.0184	0	0.0234	0.0245	0.0264
η (%)	99.92	99.89	100	99.88	99.95	99.92

3.2.5. Sensitivity Analysis

This subsection presents the sensitivity analysis performed by considering the key system variables.

Evaluation of the Curtailment Coefficient Update Period

Regarding the limiting POI power penalty system, this subsection examines the effect of the period length (W) used to calculate the curtailment coefficient (where W = 7 days is the default value in Puerto Rico). The hybrid PV–wind system, featuring a 10%/min ramp-rate limit under the 2025 Spanish spot electricity price, was evaluated by varying W from 4 to 10 days.

Figures 22 and 23 illustrate, respectively, the average curtailment factor (the mean value across all W-day periods throughout the year) and the NPV as a function of the update period length. The results demonstrate that both the average curtailment factor and the NPV increase with W.

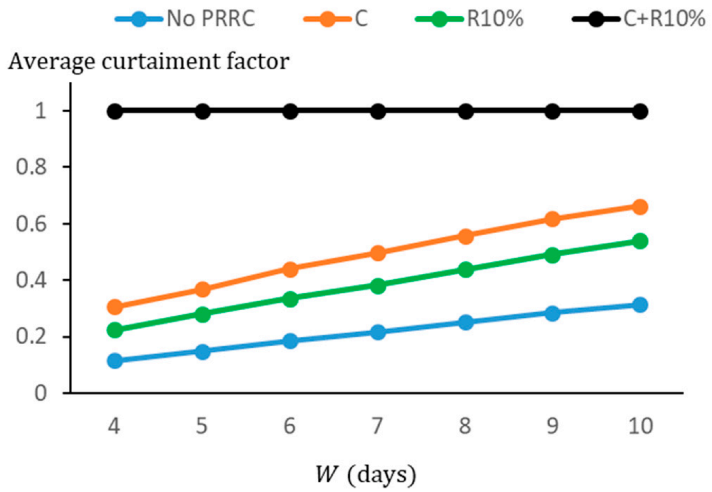


Figure 22. Average curtailment factor as a function of the update period length for hybrid PV–wind system scenarios with 10%/min ramp-rate limits, under the 2025 Spanish spot electricity price and a limiting POI power penalty system.

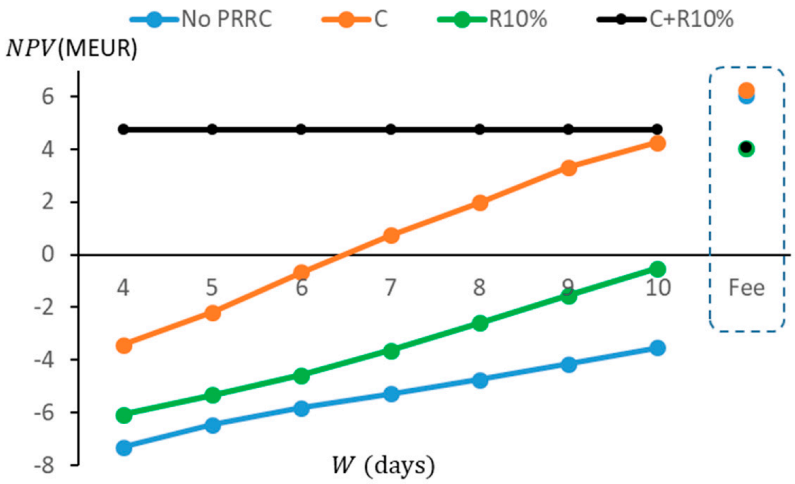


Figure 23. NPV as a function of the update period length for hybrid PV–wind system scenarios with 10%/min ramp-rate limits under the 2025 Spanish spot electricity price and a limiting POI power penalty system, including a comparison with the fee penalty system.

Furthermore, Figure 23 highlights the significant impact of W on the economic performance of the system. This figure also contrasts these outcomes with the fee penalty system, revealing that even at W = 10 days, the fee penalty system yields superior NPV results. The only exception occurs in the curtailment plus 10% reserve scenario (C+R10%), where the curtailment factor remains equal to one across all evaluated values of W. The

battery-coupled scenarios are entirely unaffected by changes in *W* because the curtailment factor for all optimal battery systems remains at one year-round.

Impact Evaluation of the Penalty Fee

Regarding the fee penalty framework, this subsection evaluates the impact of varying the penalty fee rate. The hybrid PV–wind system, subject to a 10%/min ramp-rate limit under the 2025 Spanish spot price profile, was evaluated at two alternative penalty rates (2000 EUR/MWh and 6000 EUR/MWh) to benchmark its performance against the baseline value of 4668.59 EUR/MWh. As illustrated in Figure 24, the penalty fee had the most pronounced effect on the "no PRRC" and curtailment-only scenarios. Conversely, its impact was minimal on scenarios incorporating a 10% power reserve or battery storage.

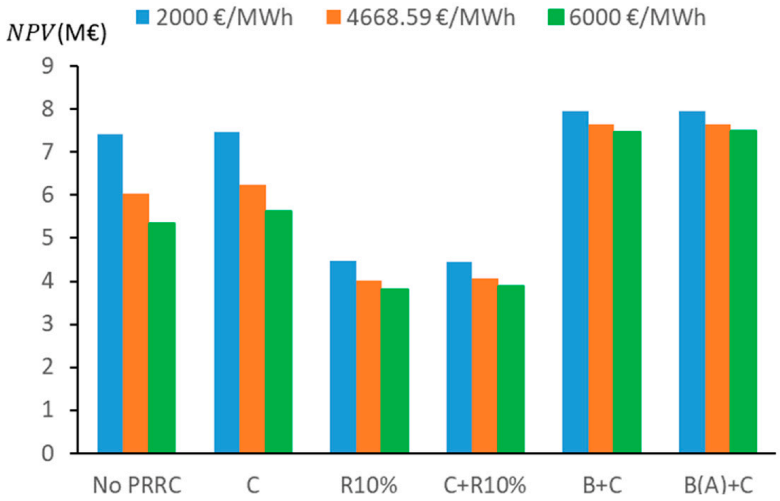


Figure 24. NPV across the different scenarios for three penalty fee cases (2000 EUR/MWh, 4668.59 EUR/MWh, and 6000 EUR/MWh) for the hybrid PV–wind system with 10%/min ramp-rate limits under the 2025 Spanish spot electricity price and a fee penalty system.

Impact of the Ramp-Rate Limit

This subsection examines the impact of varying the maximum allowable ramp-rate limit. The performance of the hybrid PV–wind system under the 2025 Spanish electricity price is compared across three different ramp rates: 5%/min, 10%/min (base case), and 20%/min.

Figure 25 presents the NPV results for the limiting POI power penalty system. The battery-coupled scenarios exhibit the highest economic performance. Interestingly, under the 20%/min ramp-rate limit, the 'No PRRC' scenario yields a superior NPV compared to the curtailment and 10% power reserve scenarios; this occurs because the curtailed energy in those configurations reduces energy revenue more severely than the cost of the avoided penalties. Conversely, for the curtailment + 10% power reserve and battery scenarios, the effect of the ramp-rate limit is almost negligible, as the curtailment factor remains at or near 1.

Figure 26 presents the NPV results for the fee penalty system, indicating that the curtailment scenario is a viable option under the 10%/min and 20%/min ramp-rate limits, while underperforming relative to the 10% reserve configuration at a 5%/min limit. Across all evaluated conditions, the battery (with curtailment) configuration consistently achieves the highest financial performance. Furthermore, the battery and the 10% power reserve scenarios exhibit minimal NPV sensitivity to ramp-rate variations due to low baseline penalty costs.

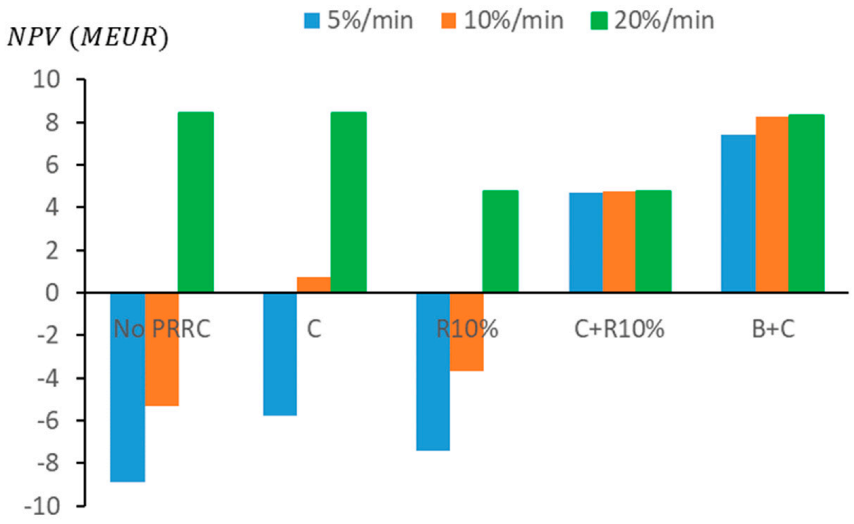


Figure 25. NPV across the different scenarios for three allowable ramp-rate limits (5%/min, 10%/min, and 20%/min) for the hybrid PV–wind system under the 2025 Spanish spot electricity price and a limiting POI power penalty system.

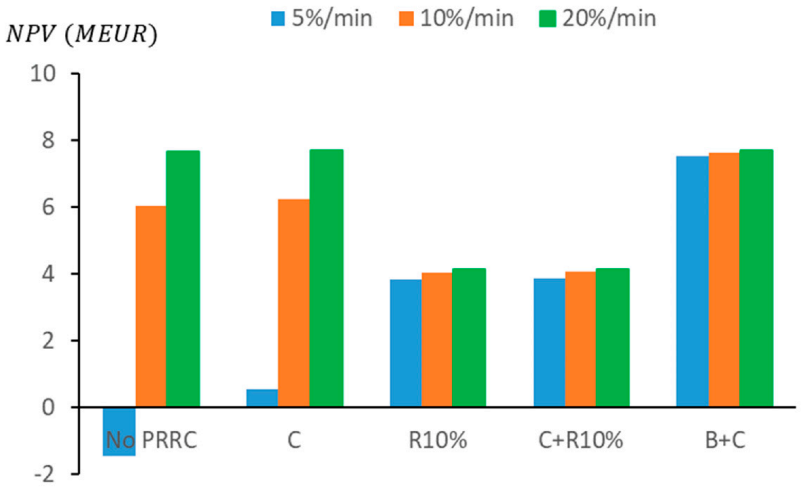


Figure 26. NPV across the different scenarios for three allowable ramp-rate limits (5%/min, 10%/min, and 20%/min) for the hybrid PV–wind system under the 2025 Spanish spot electricity price and a fee penalty system.

Impact of Time-Step Duration

This subsection evaluates the sensitivity of system performance to the time-step resolution. The behavior of the hybrid PV–wind system subject to the 2025 Spanish electricity price profile and a 10%/min ramp-rate limit is compared across three temporal resolutions: 0.5 min, 1 min (base case), and 5 min. For the 0.5 min time step, compliance with the grid-code ramp-rate limit was evaluated using a 1 min rolling window recalculated at a 30 s sampling interval. The 0.5 min irradiance and wind speed data were obtained following the same procedure described at the beginning of Section 3.2.

Figures 27–29 present the number of violations, RRC and NPV results for the POI power-limiting penalty scheme, whereas Figures 30–32 show the corresponding metrics for the fee-based penalty scheme.

Although the absolute number of violations under the 0.5 min time step is several times higher than that observed for the 1 min interval, the total number of evaluation points also doubles, resulting in comparable ramp-rate control (RRC) percentages. Conversely, with a 5 min time step, the number of violations drops below 150 across all cases, artificially yielding

an RRC near 100% and significantly higher NPV values. Consequently, using a 5 min time step is unsuitable for a grid code compliance assessment, as its lower temporal resolution fails to capture high-frequency power fluctuations. In the no-PRRC scenario under a fee-based penalty scheme, substantial discrepancies in violations, RRC, and NPV emerge when comparing 0.5 min and 1 min resolutions. Notably, the battery-assisted scenarios—as well as the curtailment scenario with a 10% power reserve—exhibit minimal NPV sensitivity to the time-step duration, whereas the remaining scenarios display substantial NPV variability.

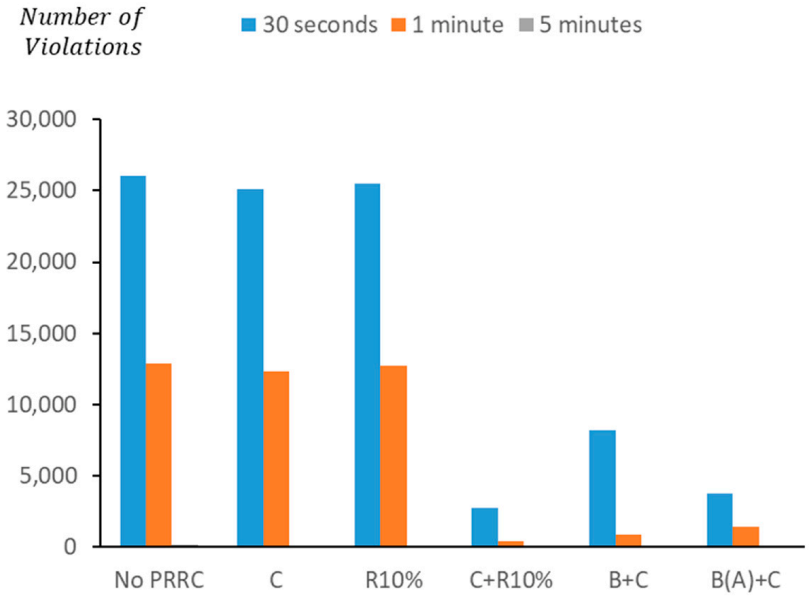


Figure 27. Number of ramp-rate violations across evaluated scenarios for three time-step resolutions (30 s, 1 min, and 5 min) in the hybrid PV–wind system under 2025 Spanish spot electricity prices and a limiting POI power penalty system.

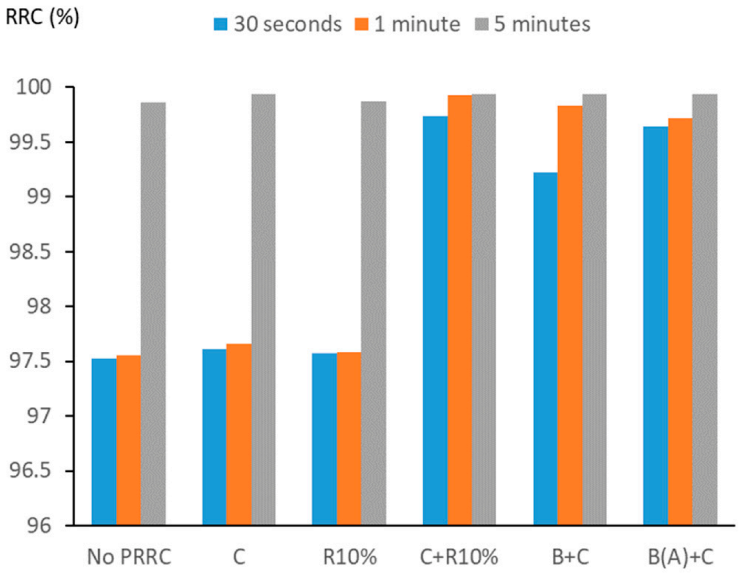


Figure 28. RRC across evaluated scenarios for three time-step resolutions (30 s, 1 min, and 5 min) in the hybrid PV–wind system under 2025 Spanish spot electricity prices and a limiting POI power penalty system.

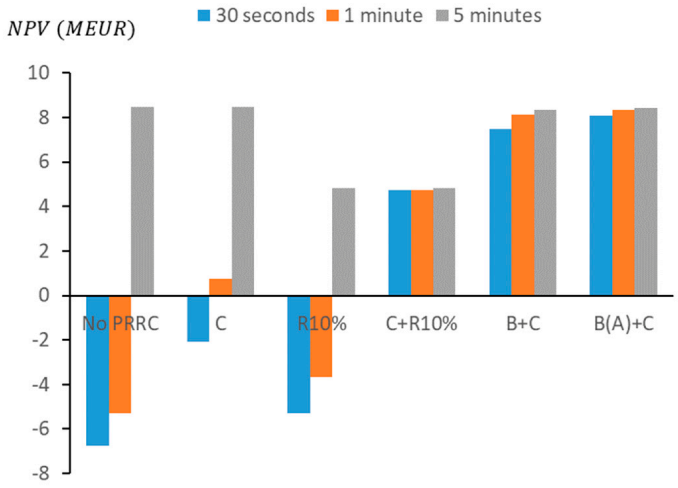


Figure 29. NPV across evaluated scenarios for three time-step resolutions (30 s, 1 min, and 5 min) in the hybrid PV–wind system under 2025 Spanish spot electricity prices and a limiting POI power penalty system.

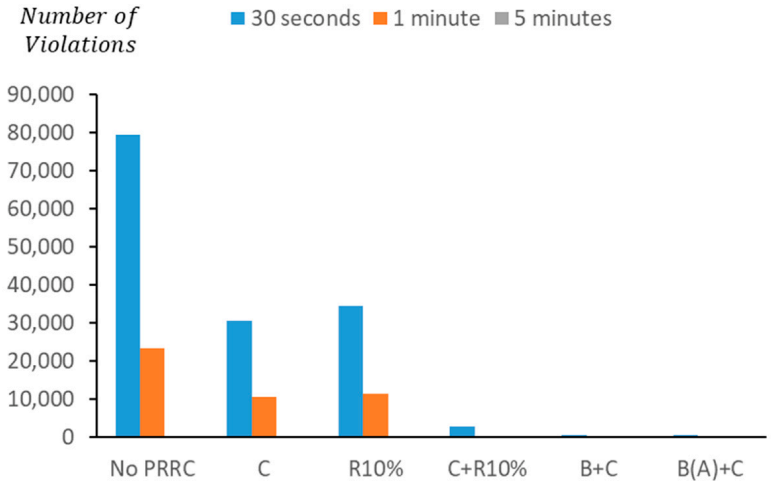


Figure 30. Number of ramp-rate violations across evaluated scenarios for three time-step resolutions (30 s, 1 min, and 5 min) in the hybrid PV–wind system under 2025 Spanish spot electricity prices and a fee-based penalty scheme.

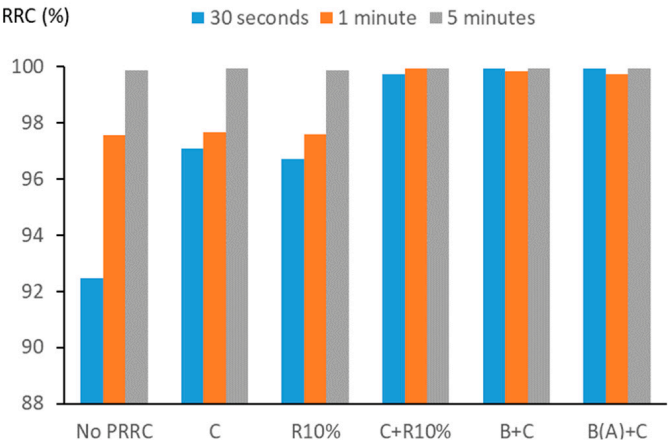


Figure 31. RRC across evaluated scenarios for three time-step resolutions (30 s, 1 min, and 5 min) in the hybrid PV–wind system under 2025 Spanish spot electricity prices and a fee-based penalty scheme.

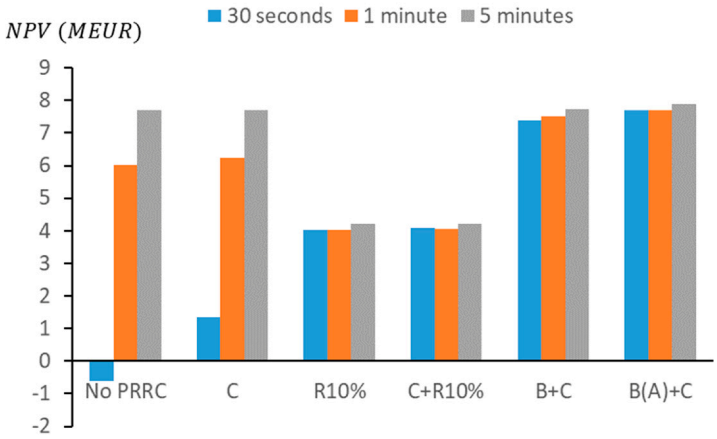


Figure 32. NPV across evaluated scenarios for three time-step resolutions (30 s, 1 min, and 5 min) in the hybrid PV–wind system under 2025 Spanish spot electricity prices and a fee-based penalty scheme.

3.2.6. Limitations of the Study

While the proposed framework effectively evaluates different PRRC techniques—including battery storage, which can also perform energy arbitrage—several methodological limitations should be acknowledged:

1. Physical Modeling of Photovoltaic and Wind Generation: The PV and wind power generation profiles were calculated using physical energy conversion models driven by meteorological time series (solar irradiance, ambient temperature, and wind speed), rather than empirical output data from operational solar and wind farms. Although physical modeling provides a standardized and reproducible baseline for optimization, real-world field measurements capture additional micro-scale dynamics, such as thermal inertia, localized cloud-edge amplification, and inverter clipping in PV systems, as well as high-frequency turbulence and spatial wind speed variations in wind farms.
2. Temporal Resolution of Input Data: The underlying meteorological datasets were obtained at an initial 10 min sampling resolution. Although shorter evaluation intervals (1 min and 0.5 min) were analyzed to assess grid code compliance, direct high-frequency field measurements recorded at 1 min or sub-minute resolution could uncover steeper instantaneous power gradients, which might slightly influence the exact ramp-rate violation metrics across the evaluated PRRC techniques.
3. Single-Year Dataset and Lack of Inter-Annual Validation: The optimization and performance evaluation rely on meteorological time series and electricity spot market prices corresponding to a single reference year (2025). Although scenario-based sensitivity checks—such as stretched price profiles and time-step duration variations—were performed to demonstrate algorithmic stability, the study does not include a multi-year inter-annual validation. As a result, long-term performance under inter-annual climate variability and evolving market conditions remains a subject for future research.

4. Conclusions

Different PRRC techniques—curtailment, power reserve, combined curtailment with power reserve, and battery with curtailment—are applied to PV, wind, and hybrid PV–wind systems. The battery and inverter–charger are optimized for: i) PRRC only or ii) PRRC combined with arbitrage. Two penalty frameworks are considered: i) limiting POI maximum power (Puerto Rico) and ii) a fee-based penalty system.

A case study in Navarra, Spain is analyzed using current costs and 2025 Spanish electricity market prices, with a 6 MW POI limit and a 10%/min ramp-rate constraint. For wind and PV–wind systems, curtailment yields better economic results than a 10% power reserve, while the opposite holds for PV systems with a fee penalty system. Combined curtailment and power reserve eliminates most violations, but reduces the injected energy and therefore the NPV.

Battery-based PRRC, with optimized battery and inverter–charger sizing, practically eliminates all violations and achieves an NPV comparable to the unconstrained case. Under the limiting POI power penalty system, the optimal battery capacity corresponds to the minimum considered value (0.1 MWh), with an operating C-rate of 2 to 4. Conversely, under the fee penalty system, both the optimal battery capacity and the C-rate are higher, ranging from 5 to 6. In all of these cases, the deployment of LTO battery technology is required.

When the battery is also utilized for arbitrage under current investment costs (75 EUR/kWh for LFP batteries, 300 EUR/kWh for LTO batteries, and 100 EUR/kW for the inverter–charger) and the 2025 Spanish market prices (assuming a 2% expected annual inflation rate), the resulting NPV improvement is negligible. This indicates that energy arbitrage is not currently financially viable in the case studied.

However, under the hypothetical stretched price curve (characterized by a much higher average price and larger daily price spreads), if the battery is also utilized for arbitrage, the optimal configurations incorporate substantial LFP battery capacities (44, 28, and 40 MWh for the PV, wind, and hybrid PV–wind systems, respectively) coupled with a 6 MW inverter–charger. The SOC operating limits for energy arbitrage span from 20% to 90%. Regarding the price thresholds for arbitrage, the upper charging limit is set to 90 EUR/MWh for the PV system and 60 EUR/MWh for the remaining configurations, whereas the lower discharging limit is 120 EUR/MWh across all cases. Relative to the unconstrained baseline, the optimal configurations incorporating battery storage for combined PRRC and arbitrage yield net present value (NPV) improvements of 17% for the wind system and 28% for the hybrid PV–wind system. Furthermore, this strategy shifts the NPV of the PV system from −2 million EUR to 6 million EUR.

A sensitivity analysis is performed considering the length of the update period for the curtailment factor (in limiting POI maximum power penalty systems), the penalty fee value (in fee penalty systems), the ramp-rate limit and the time-step duration. Across all evaluated cases, coupling a battery for PRRC is reported to achieve the highest economic performance and the lowest sensitivity to variations in these parameters.

Author Contributions: Conceptualization, R.D.-L.; methodology, R.D.-L. and J.L.B.-A.; software, R.D.-L. and J.M.L.-R.; validation, R.D.-L. and J.L.B.-A.; formal analysis, R.D.-L. and J.M.L.-R.; investigation, R.D.-L.; resources, R.D.-L.; data curation, J.M.L.-R. and J.L.B.-A.; writing—original draft preparation, R.D.-L.; writing—review and editing, J.M.L.-R. and J.L.B.-A.; visualization, R.D.-L.; supervision, J.M.L.-R.; project administration, R.D.-L. and J.L.B.-A.; funding acquisition, J.M.L.-R. All authors have read and agreed to the published version of the manuscript.

Funding: This work was supported by the Spanish Government (Ministerio de Ciencia, Innovación y Universidades—Proyectos de Generación de Conocimento 2024) under Grant PID2024-160489OBI00.

Data Availability Statement: Data available upon request.

Acknowledgments: During the preparation of this manuscript, the authors used **GitHub Copilot (latest version, GitHub Inc., San Francisco, CA, USA)**, **Claude (version 3.5 Sonnet, Anthropic, San Francisco, CA, USA)**, and **Gemini (latest version, Google LLC, Mountain View, CA, USA)** for the purposes of improving the grammar and readability of the manuscript. The authors have reviewed and edited the output and take full responsibility for the content of this publication.

Conflicts of Interest: The authors declare no conflicts of interest.

References

1. Lim, S.; Kim, T.; Lee, K.Y.; Choi, D.; Park, J. Impact of high penetration of renewables on power system frequency response: A review and verification. *Renew. Sustain. Energy Rev.* **2025**, *217*, 115728. [CrossRef]
2. Shivashankar, S.; Mekhilef, S.; Mokhlis, H.; Karimi, M. Mitigating methods of power fluctuation of photovoltaic (PV) sources–A review. *Renew. Sustain. Energy Rev.* **2016**, *59*, 1170–1184. [CrossRef]
3. Riquelme-dominguez, J.M.; García-lópez, F.D.P.; Martinez, S. Power Ramp-Rate Control via power regulation for storageless grid-connected photovoltaic systems. *Int. J. Electr. Power Energy Syst.* **2022**, *138*, 107848. [CrossRef]
4. Li, J.; Liu, B.; Wang, X.; Ma, H. Event-based optimization for smoothing ramp events in combined Wind-Storage energy systems. *Int. J. Electr. Power Energy Syst.* **2024**, *158*, 109959. [CrossRef]
5. He, Y.; Zhu, C.; Cao, C. A wind power ramp prediction method based on value-at-risk. *Energy Convers. Manag.* **2024**, *315*, 118767. [CrossRef]
6. Moore, J.; Iglesias, G. Hybridisation of offshore wind farms with floating photovoltaics: Power smoothing and output-demand divergence reduction. *Energy Convers. Manag.* **2025**, *345*, 120413. [CrossRef]
7. Yu, Y.; Guan, Y.; Tarek, B.; Andres, M.; Leon, L.; Onur, K.; Feleke, S.; Anteneh, D.; Khan, B.; Vasquez, J.C.; et al. A review of international grid codes for wind power integration. *Energy Convers. Manag. X* **2025**, *28*, 101278. [CrossRef]
8. Sukumar, S.; Marsadek, M.; Agileswari, K.R.; Mokhlis, H. Ramp-rate control smoothing methods to control output power fluctuations from solar photovoltaic (PV) sources—A review. *J. Energy Storage* **2018**, *20*, 218–229. [CrossRef]
9. Maity, S.; Rather, Z.H.; Doolla, S. A comprehensive review of grid support services from solar photovoltaic power plants. *Renew. Sustain. Energy Rev.* **2025**, *210*, 115133. [CrossRef]
10. Hassan, A.; Ahmed, J.; Papadopoulos, S.; Kahwash, F.; Goh, K. A comprehensive review of frequency response and control strategies for grid-connected solar photovoltaic systems. *Renew. Sustain. Energy Rev.* **2026**, *226*, 116324. [CrossRef]
11. Crăciun, B.I.; Kerekes, T.; Séra, D.; Teodorescu, R.; Annakkage, U.D. Power Ramp Limitation Capabilities of Large PV Power Plants with Active Power Reserves. *IEEE Trans. Sustain. Energy* **2017**, *8*, 573–581. [CrossRef]
12. Jiang, Y.; Fletcher, J.; Burr, P.; Hall, C.; Zheng, B.; Wang, D.W.; Ouyang, Z.; Lennon, A. Suitability of representative electrochemical energy storage technologies for ramp-rate control of photovoltaic power. *J. Power Sources* **2018**, *384*, 396–407. [CrossRef]
13. Montalà Palau, M.; Cheah Mañé, M.; Gomis-bellmunt, O. Techno-economic optimization for BESS sizing and operation considering degradation and ramp rate limit requirement. *J. Energy Storage* **2025**, *105*, 114631. [CrossRef]
14. Amico, G.D.; Petroni, F. Ramp Rate Limitation of Wind Power: An Overview. *Energies* **2022**, *15*, 5850. [CrossRef]
15. Frate, G.F.; Cherubini, P.; Tacconelli, C.; Micangeli, A.; Ferrari, L.; Desideri, U. Ramp rate abatement for wind power plants: A techno-economic analysis. *Appl. Energy* **2019**, *254*, 113600. [CrossRef]
16. Tadie, A.; Guo, Z.; Xu, Y. Hybrid Model-Based BESS Sizing and Control for Wind Energy Ramp Rate Control. *Energies* **2022**, *15*, 9244. [CrossRef]
17. D'Amico, G.; Petroni, F.; Vergine, S. An Analysis of a Storage System for a Wind Farm with Ramp-Rate Limitation. *Energies* **2021**, *14*, 4066. [CrossRef]
18. Benavides, D.; Arévalo, P.; Tostado-Véliz, M.; Vera, D.; Escamez, A.; Aguado, J.A.; Jurado, F. An Experimental Study of Power Smoothing Methods to Reduce Renewable Sources Fluctuations Using Supercapacitors and Lithium-Ion Batteries. *Batteries* **2022**, *8*, 228. [CrossRef]
19. Shahid, M.; Wang, D.; Zhou, X.; He, X.; Hassan, M.; Ali, A. Study of energy storage technology approaches for mitigating wind power fluctuations to enhance smart grid resilience. *Renew. Sustain. Energy Rev.* **2025**, *224*, 116072. [CrossRef]
20. Talvi, M.; Roinila, T.; Lappalainen, K. Effects of Ramp Rate Limit on Sizing of Energy Storage Systems for PV, Wind and PV–Wind Power Plants. *Energies* **2023**, *16*, 4313. [CrossRef]
21. Zhang, X.; Qin, C.; Loth, E.; Xu, Y.; Zhou, X.; Chen, H. Arbitrage analysis for different energy storage technologies and strategies. *Energy Rep.* **2021**, *7*, 8198–8206. [CrossRef]
22. Dufo-López, R. Optimisation of size and control of grid-connected storage under real time electricity pricing conditions. *Appl. Energy* **2015**, *140*, 395–408. [CrossRef]
23. Hu, Y.; Armada, M.; Jesús Sánchez, M. Potential utilization of battery energy storage systems (BESS) in the major European electricity markets. *Appl. Energy* **2022**, *322*, 119512. [CrossRef]
24. Arcos-Vargas, Á.; Canca, D.; Núñez, F. Impact of battery technological progress on electricity arbitrage: An application to the Iberian market. *Appl. Energy* **2020**, *260*, 114273. [CrossRef]
25. Terlouw, T.; AlSkaif, T.; Bauer, C.; van Sark, W. Multi-objective optimization of energy arbitrage in community energy storage systems using different battery technologies. *Appl. Energy* **2019**, *239*, 356–372. [CrossRef]
26. Dufo, R.; L.-Rojas, J.M.; Sevil, J.S.A.; Bernal, J.L. Optimising Grid-Connected PV- Battery Systems for Energy Arbitrage and Frequency Containment Reserve. *Batteries* **2024**, *10*, 427. [CrossRef]

27. Makibar, A.; Narvarte, L.; Lorenzo, E. On the relation between battery size and PV power ramp rate limitation. *Sol. Energy* **2017**, *142*, 182–193. [CrossRef]
28. Schiochet, A.F.; Duailibe Monteiro, P.R.; Borges, T.T.; Passos Filho, J.A.; de Oliveira, J.G. Photovoltaic Power Intermittency Mitigating with Battery Storage Using Improved WEEC Generic Models. *Energies* **2024**, *17*, 5166. [CrossRef]
29. Marcos, J.; De Parra, I.; Marroyo, L. A PV ramp-rate control strategy to extend battery lifespan using forecasting. *Appl. Energy* **2022**, *323*, 119546. [CrossRef]
30. Höpken, L. Reducing the Impact of Irradiance Ramps on PV Power Production–A Techno-Economic Analysis of Nowcasting. Master's Thesis, DLR-Institute of Solar Research, Cologne, Germany, 2023.
31. Manwell, J.; McGowan, J.; Rogers, A.L. *Wind Energy Explained: Theory, Design and Application*, 2nd ed.; John Wiley & Sons Ltd.: Hoboken, NJ, USA, 2009.
32. Itani, K.; De Bernardinis, A. Review on New-Generation Batteries Technologies: Trends and Future Directions. *Energies* **2023**, *16*, 7530. [CrossRef]
33. Lv, S.; Wang, X.; Lu, W.; Zhang, J. The Influence of Temperature on the Capacity of Lithium Ion Batteries with Different Anodes. *Energies* **2022**, *15*, 60. [CrossRef]
34. Downing, S.; Socie, D. Simple Rainflow Counting Algorithms. *Int. J. Fatigue* **1982**, *4*, 31–40. [CrossRef]
35. Nikolov, N.I.; Chahbaz, A.; Hildenbrand, F.; Kateri, M. Statistical investigation of temperature-dependent cycle lifetime and cell-to-cell variance in lithium-ion batteries: A model-based approach. *J. Power Sources* **2024**, *623*, 235334. [CrossRef]
36. Torre, S.; González-González, J.M.; Aguado, J.A.; Martín, S. Optimal battery sizing considering degradation for renewable energy integration. *IET Renew. Power Gener.* **2019**, *13*, 572–577. [CrossRef]
37. Fronius Solar Battery Performance. Available online: https://midsummer.ie/pdfs/fronius-performance-solar-battery.pdf (accessed on 12 December 2025).
38. Alam, M.J.E.; Saha, T.K. Cycle-Life Degradation Assessment of Battery Energy Storage Systems Caused by Solar PV Variability. In Proceedings of the 2016 IEEE Power and Energy Society General Meeting, Boston, MA, USA, 17–21 July 2016; pp. 1–5. [CrossRef]
39. PowerTech Batteries. Available online: https://www.powertechsystems.eu (accessed on 10 February 2026).
40. Petit, M.; Prada, E.; Sauvant-Moynot, V. Development of an empirical aging model for Li-ion batteries and application to assess the impact of Vehicle-to-Grid strategies on battery lifetime. *Appl. Energy* **2016**, *172*, 398–407. [CrossRef]
41. Naumann, M.; Schimpe, M.; Keil, P.; Hesse, H.C.; Jossen, A. Analysis and modeling of calendar aging of a commercial $LiFePO_4$/graphite cell. *J. Energy Storage* **2018**, *17*, 153–169. [CrossRef]
42. Lee, J.; Choi, K.; Lee, W.; Lee, S.; Yoon, J. Quantitative lifetime prediction and operating window identification for $Li_4Ti_5O_{12}$-based batteries under coupled thermal and rate stress. *J. Energy Storage* **2026**, *182*, 124853. [CrossRef]
43. Dubarry, M.; Devie, A. Battery durability and reliability under electric utility grid operations: Representative usage aging and calendar aging. *J. Energy Storage* **2018**, *18*, 185–195. [CrossRef]
44. Dubarry, M.; Qin, N.; Brooker, P. Calendar aging of commercial Li-ion cells of different chemistries–A review. *Curr. Opin. Electrochem.* **2018**, *9*, 106–113. [CrossRef]
45. Stroe, A.I.; Stroe, D.L.; Knap, V.; Swierczynski, M.; Teodorescu, R. Accelerated Lifetime Testing of High Power Lithium Titanate Oxide Batteries. In Proceedings of the 2018 IEEE Energy Conversion Congress and Exposition, Portland, OR, USA, 23–27 September 2018; pp. 3857–3863. [CrossRef]
46. National Solar Radiation Database (NSRDB). National Laboratory of the Rockies. U.S. Department of Energy. Available online: https://nsrdb.nlr.gov/ (accessed on 20 December 2025).
47. Govierno de Navarra. Meteorología y Climatología de Navarra (Meteorology and Climatology of Navarre, Spain). Available online: https://meteo.navarra.es/estaciones/mapadeestaciones.cfm (accessed on 12 December 2025).
48. Caldas, M.; Alonso-Suarez, R. Very short-term solar irradiance forecast using all-sky imaging and real-time irradiance measurements. *Renew. Energy* **2019**, *143*, 1643–1658. [CrossRef]
49. Reindl, D.T.; Beckman, W.A.; Duffie, J.A. Evaluation of hourly tilted surface radiation models. *Sol. Energy* **1990**, *45*, 9–17. [CrossRef]
50. Crawford, A.; Wu, D.; Viswanathan, V.; Balducci, P.; Vartanian, C.; Hardy, T.; Alam, J.; Mongird, K. Washington Clean Energy Fund: Energy Storage System Consolidated Performance Test Results. 2020. Available online: https://www.osti.gov/servlets/purl/1602252 (accessed on 20 May 2025).
51. International Renewable Energy Agency. Renewable Generation Costs in 2024. 2024. Available online: https://www.irena.org/-/media/Files/IRENA/Agency/Publication/2025/Jul/IRENA_TEC_RPGC_in_2024_2025.pdf (accessed on 9 March 2026).
52. Rangelova, K.; Jones, D. How Cheap Is Battery Storage? 2025. Available online: https://ember-energy.org/latest-insights/how-cheap-is-battery-storage/#3-with-a-65-mwh-lcos-shifting-half-of-daily-solar- (accessed on 23 December 2025).
53. Lithium Titanate Oxide Battery Market Size & Share Analysis-Growth Trends and Forecast (2025–2030). Available online: https://www.mordorintelligence.com/industry-reports/lithium-titanate-oxide-battery-market (accessed on 5 June 2026).

54. Cole, W.; Ramasamy, V.; Turan, M.; Cole, W.; Ramasamy, V.; Turan, M. *Cost Projections for Utility-Scale Battery Storage: 2025 Update*; National Renewable Energy Laboratory (NREL): Golden, CO, USA, 2025.
55. Bernal-Agustín, J.L.; Dufo-López, R. Efficient design of hybrid renewable energy systems using evolutionary algorithms. *Energy Convers. Manag.* **2009**, *50*, 479–489. [CrossRef]
56. Javed, M.S.; Ma, T.; Jurasz, J.; Ahmed, S.; Mikulik, J. Performance comparison of heuristic algorithms for optimization of hybrid off-grid renewable energy systems. *Energy* **2020**, *210*, 118599. [CrossRef]

Disclaimer/Publisher's Note: The statements, opinions and data contained in all publications are solely those of the individual author(s) and contributor(s) and not of MDPI and/or the editor(s). MDPI and/or the editor(s) disclaim responsibility for any injury to people or property resulting from any ideas, methods, instructions or products referred to in the content.